

# Geochemistry, Geophysics, Geosystems

## RESEARCH ARTICLE

10.1029/2020GC008946

### Key Points:

- Back-arc rifting is initiated by tectonic rather than magmatic processes
- Back-arc magmas form by decompression melting with little influence of a slab component
- Arc front magmas form from flux melting containing variable slab components reflecting different input from the slab

### Supporting Information:

- Supporting Information S1

### Correspondence to:

K. M. Haase,  
Karsten.Haase@fau.de

### Citation:

Haase, K. M., Gress, M. U., Lima, S. M., Regelous, M., Beier, C., Romer, R. L., & Bellon, H. (2020). Evolution of magmatism in the New Hebrides Island Arc and in initial back-arc rifting, SW Pacific. *Geochemistry, Geophysics, Geosystems*, 21, e2020GC008946. <https://doi.org/10.1029/2020GC008946>

Received 27 JAN 2020

Accepted 21 JUL 2020

Accepted article online 4 SEP 2020

©2020. The Authors.

This is an open access article under the terms of the Creative Commons Attribution License, which permits use, distribution and reproduction in any medium, provided the original work is properly cited.

## Evolution of Magmatism in the New Hebrides Island Arc and in Initial Back-Arc Rifting, SW Pacific

K. M. Haase<sup>1</sup> , M. U. Gress<sup>2</sup> , S. M. Lima<sup>1</sup>, M. Regelous<sup>1</sup>, C. Beier<sup>1,3</sup> , R. L. Romer<sup>4</sup>, and H. Bellon<sup>5</sup>

<sup>1</sup>GeoZentrum Nordbayern, Friedrich-Alexander-Universität Erlangen-Nürnberg, Erlangen, Germany, <sup>2</sup>Geology and Geochemistry Cluster, VU University, Amsterdam, The Netherlands, <sup>3</sup>Department of Geosciences and Geography, Research Programme of Geology and Geophysics (GeoHel), University of Helsinki, Helsinki, Finland, <sup>4</sup>Deutsches GeoForschungsZentrum (GFZ), Potsdam, Germany, <sup>5</sup>Laboratoire de Géochimie, Université de Bretagne Occidentale, Brest, France

**Abstract** We present new geochemical and isotopic data for rock samples from two island arc volcanoes, Erromango and Vulcan Seamount, and from a 500 m thick stratigraphic profile of lava flows exposed on the SW flank of Vate Trough back-arc rift of the New Hebrides Island Arc (NHIA). The basalts from the SW rift flank of Vate Trough have ages of ~0.5 Ma but are geochemically similar to those erupting along the active back-arc rift. The weak subduction component in the back-arc basalts implies formation by decompression melting during early rifting and rifting initiation by tectonic processes rather than by lithosphere weakening by arc magma. Melting beneath Vate Trough is probably caused by chemically heterogeneous and hot mantle that flows in from the North Fiji Basin in the east. The melting zone beneath Vate Trough back-arc is separate from that of the arc front, but a weak slab component suggests fluid transport from the slab. Immobile incompatible element ratios in South NHIA lavas overlap with those of the Vate Trough depleted back-arc basalts, suggesting that enriched mantle components are depleted by back-arc melting during mantle flow. The slab component varies from hydrous melts of subducted sediments in the Central NHIA to fluids from altered basalts in the South NHIA. The volcanism of Erromango shows constant compositions for 5 million years, that is, there is no sign for variable depletion of the mantle or for a change of slab components due to collision of the D'Entrecasteaux Ridge as in lava successions further north.

## 1. Introduction

Subduction zones are dynamic plate boundaries where oceanic lithosphere is subducted into the Earth's mantle causing stress in the upper plate and flow of the asthenosphere (e.g., Heuret & Lallemand, 2005; Uyeda & Kanamori, 1979; Wiens et al., 2008). Volcanism occurs at oceanic island arcs and frequently at extensional back-arc basins where the magmas form by hydrous flux melting due to water transfer from the subducting slab into the mantle wedge and/or by adiabatic melting of ascending mantle (Conder et al., 2002; Grove et al., 2012; Kushiro, 1990). Corner flow in the asthenospheric mantle wedge causes transport of material from the back-arc to the arc (Wiens et al., 2008), and partial melting beneath the back-arc probably depletes the upper mantle in many subduction systems so that island arc lavas have lower concentrations of fluid-immobile elements like Nb, Zr, and Ti than back-arc basalts (e.g., Kincaid & Hall, 2003; McCulloch & Gamble, 1991; Woodhead et al., 1993). On the other hand, subduction of altered basalts and of sediments release hydrous fluids and melts into the mantle wedge, affecting melting processes and the incompatible element compositions of the arc and back-arc magmas (McCulloch & Gamble, 1991; Plank & Langmuir, 1993; Saunders & Tarney, 1979). The compositions of back-arc lavas thus range from being similar to mid-ocean ridge basalts (MORB) to those typically found at island arcs (Pearce et al., 1995). The extensional forces within the arc lithosphere are poorly understood and potential mechanisms for extension may be the motion of the upper plate, slab rollback of the subducting plate, or asthenospheric mantle flow (e.g., Billen, 2017; Heuret & Lallemand, 2005; Karig, 1974; Sleep & Toksöz, 1971; Tamaki, 1985). Arc rifting can occur between the fore-arc and back-arc (Martinez & Taylor, 2006), and it has been proposed that the ascent of arc magmas may weaken the lithosphere causing rifting (Molnar & Atwater, 1978). The melts beneath island arc/back-arc systems possibly rise as diapirs of partially molten mantle rocks that may

consist of mixtures between peridotite, sediments, and metasomatized hydrous peridotite (Gerya & Yuen, 2003; Hall & Kincaid, 2001; Hasenclever et al., 2011; Sleeper & Martinez, 2014). Thus, the magmatic rocks recovered at subduction zones are highly variable and reflect the geodynamic situation at the time of formation, for example, the location of the magma system relative to the slab and mantle wedge.

Here we provide new geochemical and isotopic data on basaltic rocks from two volcanoes (Erromango and Vulcan Seamount) of the New Hebrides Island Arc (NHIA) front and from the rifted flank of the young Vate Trough back-arc basin that yield insights into early stages of island arc rifting and magma genesis. The uppermost 500 m of lavas exposed on the SW rift flank are younger than 0.5 Ma and resemble the basalts of the Vate Trough axis, implying that the present basin formed within a few 100 kyr, and the Vate Trough magmas formed by decompression melting without a significant slab component. The lavas of the South NHIA are generally more depleted than those of the Central NHIA, probably reflecting prior melting in the back-arc of the Coriolis Troughs. The South NHIA magmas formed from a mantle wedge metasomatized by hydrous fluids from altered basalts, whereas the Central NHIA magmas indicate a hydrous melt from subducted sediment in their mantle source. New data on the arc front island of Erromango suggest that magma sources and melting have remained constant over the past 5 Ma, although the volcanism apparently has migrated away from the trench.

## 2. Geological Setting of the New Hebrides Island Arc (NHIA)

Volcanism in the NHIA occurs between 13°S and 21°S on the New Hebrides ridge (Schellart et al., 2006), and volcanic activity is also observed in the back-arc basins of the Jean Charcot Troughs in the north (Figure 1a) and the Coriolis Troughs behind the South NHIA (Maillet et al., 1995). The New Hebrides Ridge represents an old island arc that formed along the Vitiac Trench since the Late Oligocene (Schellart et al., 2006). The rollback of the subducting Australian-Indian Plate initiated clockwise rotation along the NHIA and is responsible for the wedge-shaped opening of the North Fiji back-arc basin (Figure 1a) where spreading commenced 12 to 11 million years ago (Pelletier et al., 1998; Schellart et al., 2006). Subduction of the Australian-Indian Plate beneath the Pacific Plate since ~10 Ma formed the volcanoes of the present NHIA between 13°S and 21°S, most of which are active, although some are extinct since the Pleistocene (Gorton, 1977; Maillet et al., 1995; Peate et al., 1997). The most recent volcanic period formed the arc front islands of Aoba, Ambrym, Epi, Efate, Erromango, Tanna, and Anatom, but the active volcanoes (<1 Ma old) frequently lie on the eastern sides of the islands (Figures 1a and 1b). Present convergence rates at the southern NHIA range from 90 mm/year at Efate to 120 mm/year at Erromango (Bergeot et al., 2009), whereas back-arc opening in the Coriolis Troughs occurs at ~30 mm/year with a significant left-lateral strike-slip motion (Pelletier et al., 1998). Measurements by GPS indicate that the upper plate of the southern NHIA between 17°S and 20°S is advancing at 90 to 120 mm/year relative to a fixed Australian Plate (Bergeot et al., 2009). The upper plate of the NHIA is advancing toward the west, which is explained by westward-directed mantle flow from the North Fiji Basin (Heuret & Lallemand, 2005).

The collision of the D'Entrecasteaux Ridge (Figure 1a) with the NHIA 2 to 3 million years ago caused uplift of the central part of the New Hebrides ridge and clockwise arc rotation and opening of the young Coriolis back-arc basins (Bergeot et al., 2009; Wallace et al., 2009). The collision occurred initially at the latitude of Epi island and migrated northward (Greene & Collot, 1994). Compression in the upper plate apparently affects magma ascent and the location of volcanic centers as far south as the Epi volcanoes (Beier et al., 2018). A significant change in Sr and Pb isotope compositions occurs in lavas along the arc front where volcanoes of the Central NHIA north of 17.5°S (Efate, Epi, Ambrym, Aoba, and Gaua) erupted lavas with  $^{87}\text{Sr}/^{86}\text{Sr} > 0.7036$  (Figure 2a) and lower  $^{206}\text{Pb}/^{204}\text{Pb}$  than volcanoes of Erromango, Tanna, and Anatom from the South NHIA (Briqueu et al., 1994; Crawford et al., 1995; Laporte et al., 1998; Peate et al., 1997). Because Central NHIA lavas older than ~2 Ma resemble those from the South NHIA, it was suggested that the change in isotopic compositions was caused by the collision of the D'Entrecasteaux ridge with the NHIA (Briqueu et al., 1994; Crawford et al., 1995). Whereas the lavas of the South NHIA and the Central NHIA prior to the collision show a Pacific MORB-type source in terms of Pb isotope compositions, the young Central NHIA lavas indicate melting of an Indian Ocean-type source (Crawford et al., 1995; Peate et al., 1997). Most lavas from the entire NHIA as well as those from the North Fiji Basin have relatively low Nd isotope ratios at a given Hf isotope composition and resemble Indian Ocean MORB (Pearce et al., 2007). Pacific

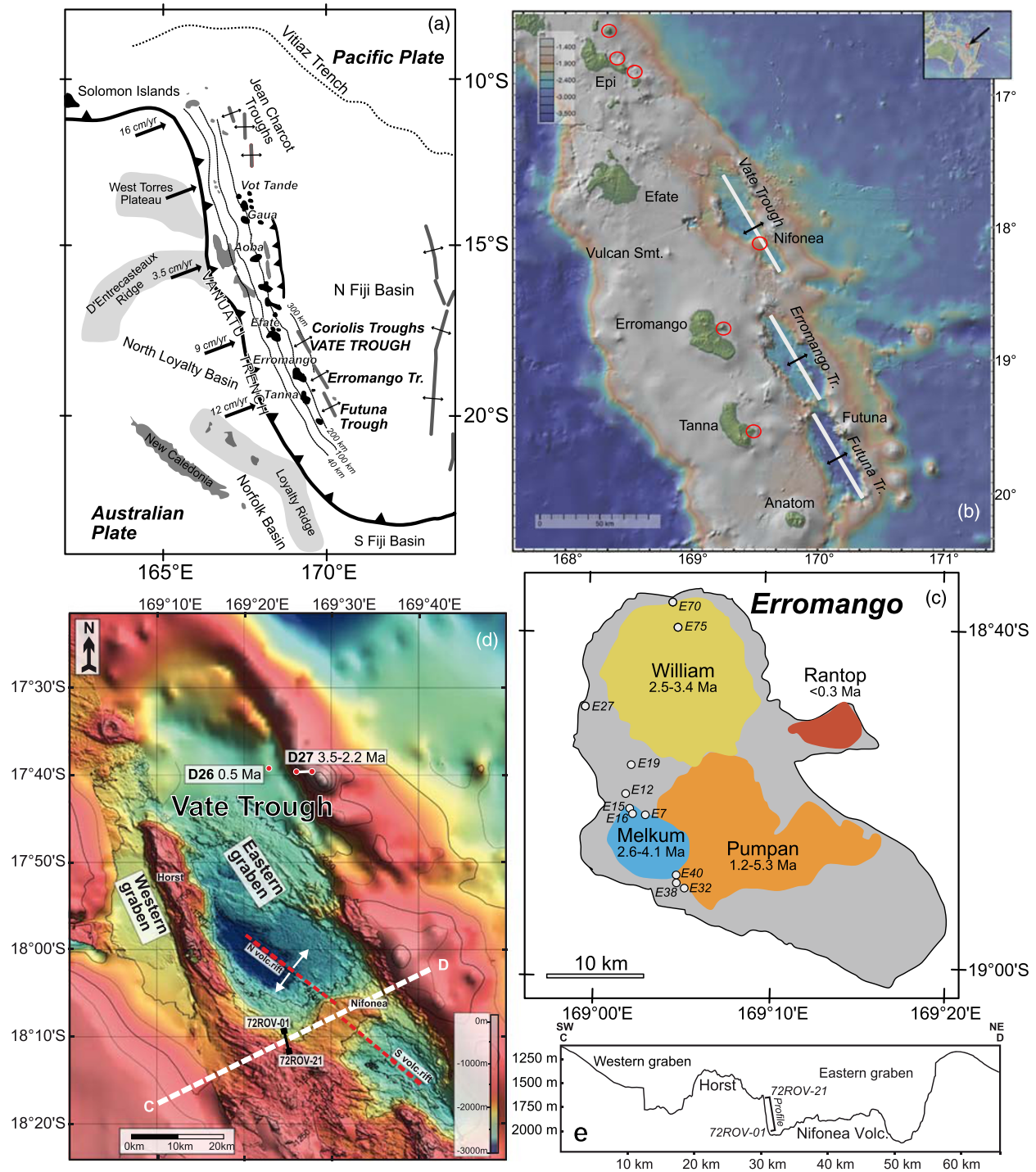


**Figure 1.** (a) Sketch map of the New Hebrides Island Arc (NHIA) and the North Fiji Basin showing the most important tectonic features and the young arc volcanoes in black. The West Torres Plateau as well as the D'Entrecasteaux and Loyalty Ridges are major shallow structures in the North Loyalty, Norfolk, and South Fiji Basins that are subducted in the Vanuatu Trench. Behind the arc front, consisting of the islands of Aoba, Ambrym, Epi, Eate, Erromango, Tanna, and Anatom, young back-arc rifts are opening along the Jean Charcot Troughs in the north and along the Vate Trough (VT), the Erromango Trough (ET), and the Futuna Trough (FT) in the south. The depths of the subducting slab are indicated by the thin black lines and show that the slab lies more than 240 km deep beneath the Vate Trough. (b) Bathymetric map from GeoMapApp showing the Coriolis Troughs and the island arc front. Red circles show young (active) volcanic edifices. (c) Geological map of Erromango island after Bellon et al. (1984) showing the older volcanic formations and the sample locations. (d) Bathymetric map of Vate Trough with the central horst structure in the basin and the location of the sampling profile. Also shown are sampling locations of previously age-dated samples at the NE flank of Vate Trough (Monjaret et al., 1991). Solid black line indicates location of sampled profile 72ROV; dotted white line marks cross-section (c) and (d) through the Vate Trough shown in (e).

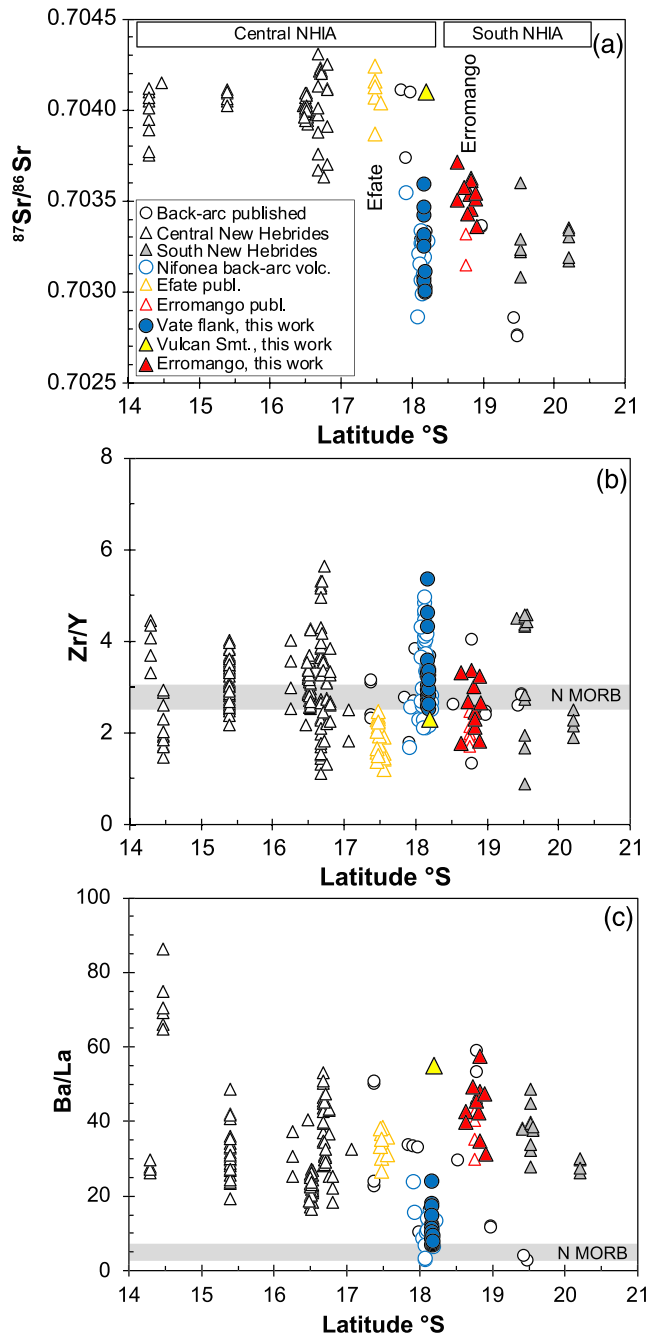


**Figure 2.** Variation of the (a) Sr isotope, (b) Zr/Y, and (c) Ba/La compositions of lavas from the island arc front and the back-arc. Data are from this work and Barsdell and Berry (1990), Barsdell et al. (1982), Beaumais et al. (2013), Beier et al. (2018) Dupuy et al. (1982), Eggins (1993), Gorton (1977), Laporte et al. (1998), Lima et al. (2017), Marcelot et al. (1983), Mailliet et al. (1995), Peate et al. (1997); Métrich et al. (2011), Raos and Crawford (2004), Robin et al. (1994), Sorbadere et al. (2013).

and Indian MORB-type mantle sources were suggested by parallel mixing trends with slab components in U series isotopes (Turner et al., 1999). The occurrence of the Indian Ocean-type mantle source was explained with inflow from the North Fiji Basin some 2 to 3 Ma ago and upwelling of this mantle beneath the young back-arc regions (Briqueu et al., 1994; Crawford et al., 1995; Heyworth et al., 2011; Pearce et al., 2007; Peate et al., 1997).

Vate Trough is the northernmost rift basin, some 50 km east of the island arc front volcanoes of Efate, Vulcan Seamount, and Erromango of which only Erromango shows active volcanism (Figures 1b and 1c). Seismic data suggest a crustal thickness of about 28 km beneath Erromango but only about 12 km beneath the back-arc (Ibrahim et al., 1980). The island Erromango lies on a 1,400 m high volcanic structure with a diameter of ~75 km. Four older volcanic units are defined on the island (Figure 1c) and have K-Ar ages between 5.3 and 1.1 Ma, whereas the youngest activity occurs at Mt. Rantop on the east coast of Erromango with ages <0.3 Ma (Bellon et al., 1984). Vulcan Seamount is a small volcanic structure between Erromango and Efate with a height of 1,000 m and a diameter of 15 km (Figure 1b). The island of Efate further north rises some 1,600 m from the New Hebrides ridge and has a diameter of ~95 km. The island is largely covered by an ~1 Ma old pumice formation and younger mafic lavas occur in the northernmost part of Efate and on three small islands in the north (Raos & Crawford, 2004).

The Coriolis Troughs include three extensional intra-arc basins: Vate, Erromango, and Futuna Troughs, which lie 30 to 50 km east of the volcanic front of the South NHIA (Figure 1b). Young volcanism is only known from Vate and Futuna Troughs (Lima et al., 2017; Mailliet et al., 1995; Monjaret et al., 1991). Vate Trough (Figure 1d) is ~70 km long and up to 20 km wide with a maximum water depth of ~2,800 m and consists of a complex NNW-SSE-trending double graben (Anderson et al., 2016; Mailliet et al., 1995) with a horst at 1,200 m water depth separating a small western graben (mean depth ~2,150 m) from a larger and deeper eastern graben (mean depth ~2,550 m). The southern part of Vate Trough is dominated by the ~1,000 m high Nifonea volcano and its two volcanic rift zones (Figure 1e), whereas the northern part of the basin comprises elongated, NW striking ridges with small volcanic structures (Anderson et al., 2016). The slab beneath Vate Trough dips with angles between 40°–60° and lies at 240–300 km depth (Figure 1a) with few deep earthquakes occurring beneath the back-arc rift (Baillard et al., 2015; Hayes et al., 2012). The shallower depth of the Vate Trough compared to the other troughs may reflect thermal uplift that is consistent with recent, extensive volcanism and hydrothermal venting at Nifonea volcano (Lima et al., 2017; McConachy et al., 2005). The Nifonea lavas range in composition from basalt to basaltic trachyandesite and show incompatible element-enriched compositions, in which the youngest lavas are the most enriched, indicating that the most

recent melts formed from the most enriched mantle source with the most radiogenic Sr and Pb isotope ratios (Lima et al., 2017). Potassium-Ar dating of crustal rocks dredged along the NE Vate Trough rift flanks (Figure 1d) at 1,960 to 600 m depth (D27-29) revealed ages of 3.7 to 2.2 Ma (Monjaret et al., 1991). Most of these samples are high-K dacites, but two basalts have ages of 3.5 to 3.2 Ma. Two dacite samples dredged

from the floor of Vate Trough at 2,080 to 1,850 m depth (D26, Figure 1d) were dated at 0.5 to 0.4 Ma (Monjaret et al., 1991).

### 3. Sampling and Analytical Methods

In this work we analyzed 11 fresh lavas from Erromango with ages between 5.3 and 1.1 Ma that have been described and age-dated earlier (Bellon et al., 1984). Additionally, we sampled a small volcano (Vulcan Seamount according to Monzier et al., 1997) in the arc front between Erromango and Efate with a TV-guided grab and recovered Mn-oxide-crusting lava (2TVG). In the back-arc, 21 rock samples (72ROV01 to -21) were recovered (Figure 1d) along a 500 m vertical crustal profile exposed at the western rift flank of Vate Trough using the remotely operated vehicle (ROV) Kiel 6000 of the GEOMAR Helmholtz Centre for Ocean Research Kiel during RV Sonne cruise SO229 in 2013. Lavas were sampled between 1,991 and 1,506 m water depth (Table S1) using the hydraulic arms of the ROV. In order to obtain a consistent stratigraphy for the uppermost part of the crust, only in situ lava samples were recovered and dikes were avoided based on outcrop observations. On board, the rock samples were described petrographically and cut to retrieve pieces for thin-sections and fresh cores; volcanic glass rims were separated and handpicked to exclude altered material.

Olivine, clinopyroxene and plagioclase were analyzed with a JEOL JXA-8200 Superprobe electron microprobe at the GeoZentrum Nordbayern operated with an acceleration voltage of 15 kV, a beam current of 15 nA, and a defocused beam of 3  $\mu\text{m}$  in diameter. Fresh volcanic glasses of four samples from the back-arc were embedded in epoxy and polished to determine major elements,  $\text{SO}_3$  and Cl concentrations using the JEOL JXA-8200 Superprobe electron microprobe following the methods in Brandl et al. (2012). The analyses were performed using an acceleration voltage of 15 kV, a beam current of 15 nA and a defocused beam of 10  $\mu\text{m}$  in diameter. The reproducibility of the method was checked by periodic analyses of VG-2, VG-99, and VG-568 standards, and the average concentrations obtained for VG-2 are shown in the supporting information Table S1. The data for the volcanic glasses (Table S1) represent averages of 10 individual spot analyses of a single glass chip.

Fresh cores of whole-rock samples were washed with deionized water, dried at 40°C, coarse crushed and ground in a vibratory agate disc mill. The powders were used to produce fused glass beads. Major element oxides and selected trace elements (Ba, Cr, Ga, Nb, Ni, Rb, Sr, V, Y, Zn, and Zr) were determined on a Spectro Xepos Plus XRF spectrometer at the GeoZentrum Nordbayern. Loss on ignition (LOI) was determined by weighing ~1 g of sample before and after drying in a muffle furnace at 1050°C for 12 hr. Precision and accuracy were checked (Table S1) by analyses of the basalt standards BE-N ( $n = 3$ ) and BR ( $n = 2$ ) and are better than 2.5% for all major elements except P (9%). Trace element measurements were carried out using a Thermo Scientific X-Series 2 Quadrupole Inductively Coupled Plasma Mass Spectrometer (ICP-MS) at the GeoZentrum Nordbayern. Sample solutions (dilution factor of 4,000) were introduced into the plasma via an Aridus desolvating nebulizer to minimize molecular interferences and mixed online with a Be, In, Rh, and Bi internal standard solution in order to correct for instrument drift. Reproducibility and accuracy were monitored by periodic analyses of BHVO-2 standard (Table S1) and is generally better than 5%. Accuracy relative to GEOREM preferred concentrations for BHVO-2 is within 3%, except for Cs (10%).

The Sr isotope ratios of the lavas from the Vate Trough flank were analyzed after leaching samples in 2.5 N HCl for 1 hr at 100°C on a Thermo MAT-262 TIMS at Vrije Universiteit Amsterdam. The  $^{87}\text{Sr}/^{86}\text{Sr}$  data were normalized with  $^{86}\text{Sr}/^{88}\text{Sr} = 0.1194$ . The long-term  $^{87}\text{Sr}/^{86}\text{Sr}$  value of Sr reference material NIST SRM 987 was  $0.710270 \pm 0.000010$  ( $2\sigma$ ,  $n = 20$ ), and analyses are reported relative to a value of 0.710250 for the NBS987 standard. Total procedural blanks are less than 100 pg for Sr. The Nd and Pb isotope compositions of the lavas from the flank of Vate Trough were determined on unleached samples on a Thermo Fisher TRITON thermal ionization multicollector mass spectrometer at the Deutsches GeoForschungszentrum GFZ (Potsdam) following the procedure in Romer et al. (2001). The Nd isotopic composition was determined using dynamic multicollection; the data are normalized relative to  $^{146}\text{Nd}/^{144}\text{Nd} = 0.7219$ . The long-term reproducibility of the La Jolla Nd reference material was  $0.511855 \pm 0.000006$  ( $2\sigma$  for  $n = 14$  analyses) for  $^{143}\text{Nd}/^{144}\text{Nd}$ . Analytical uncertainties of the individual measurements are reported as  $2\sigma_m$ . Total procedural blanks are less than 30 pg Nd. Instrumental fractionation was corrected with 0.1% amu, as determined from repeated measurement of lead reference-material NIST SRM 981. Accuracy and precision of reported

Pb-ratios are better than 0.1% at the 2-sigma level. Total procedural blanks for whole-rock samples are better than 15–30 pg Pb.

Strontium, Nd, and Pb isotope ratios of the Erromango samples and sample 002TVG-01 were determined at the GeoZentrum Nordbayern after leaching of the sample for 1 hr in HCl following the separation methods described previously (Haase et al., 2019). The Sr and Nd isotope measurements were carried out on a Thermo Fisher TRITON thermal ionization multicollector mass spectrometer in static mode at the GeoZentrum Nordbayern, Friedrich-Alexander-Universität Erlangen-Nürnberg, Germany. Strontium isotope measurements were corrected for instrumental mass fractionation assuming  $^{88}\text{Sr}/^{86}\text{Sr} = 0.1194$ . Neodymium isotope data were corrected for mass fractionation using a  $^{146}\text{Nd}/^{144}\text{Nd}$  ratio of 0.7219. Samarium interference on masses 144, 148, and 150 was corrected by measuring  $^{147}\text{Sm}$ . The average value of the NIST SRM 987 Sr standard during this study was 0.710259, and an in-house Nd standard solution gave  $^{143}\text{Nd}/^{144}\text{Nd}$  of 0.511840, equivalent to a value of 0.511850 for the La Jolla standard. Sr isotope data are reported relative to a value of 0.710250 for the NBS987 standard. Lead isotope measurements were carried out on a Thermo Fisher NEPTUNE MC-ICP-MS using a  $^{207}\text{Pb}/^{204}\text{Pb}$  double spike to correct for instrumental mass fractionation. The double spike, with a  $^{207}\text{Pb}/^{204}\text{Pb}$  ratio of 0.813508, was calibrated against a solution of NIST SRM 982 equal atom Pb standard. Samples were diluted with 2%  $\text{HNO}_3$  to a concentration of approximately 20 ppb, and an aliquot of this solution was spiked in order to obtain a  $^{208}\text{Pb}/^{204}\text{Pb}$  ratio of about 1. Spiked and unspiked sample solutions were introduced into the plasma via a Cetac Aridus desolvating nebulizer, and measured in static mode. Interference of  $^{204}\text{Hg}$  on mass 204 was corrected by monitoring  $^{202}\text{Hg}$ . An exponential fractionation correction was applied offline using the iterative method of Compston and Oversby (1969), the correction was typically 4.5 permil per amu. Eight measurements of the NIST SRM 981 Pb isotope standard (measured as an unknown) over the course of this study gave  $^{206}\text{Pb}/^{204}\text{Pb}$ ,  $^{207}\text{Pb}/^{204}\text{Pb}$ ,  $^{208}\text{Pb}/^{204}\text{Pb}$  ratios of  $16.9408 \pm 0.0018$ ,  $15.4993 \pm 0.0019$ , and  $36.7244 \pm 0.0036$ , respectively. Typical procedural blanks for Pb, Sr, and Nd were 30, 200, and 80 pg, respectively.

The lava sample 072ROV-04 was selected for groundmass  $^{40}\text{Ar}/^{39}\text{Ar}$  age dating at Oregon State University (OSU), USA, following the method outlined in Koppers et al. (2011), and yielded a plateau age of  $510.8 \pm 27.3$  kyr and an isochron age of  $508.3 \pm 41.8$  kyr (Table S2). The clean sample was crushed using a steel plated jaw crusher and the grain size fraction between 150–300  $\mu\text{m}$  sieved and washed. The fraction was acid-leached with 1 M HCl, then 6 M HCl, 1 M  $\text{HNO}_3$ , 3 M  $\text{HNO}_3$ , and ultra-pure deionized water (all for about 60 min) in an ultrasonic bath heated to  $\sim 50^\circ\text{C}$ . The leached sample was irradiated for 6 hr in the TRIGA nuclear reactor at OSU, together with the FCT NM sanidine flux monitor (Kuiper et al., 2008). The individual J-values for each samples were calculated by parabolic extrapolation of the measured flux gradient against irradiation height and typically give 0.1–0.2% uncertainty ( $1\sigma$ ). The  $^{40}\text{Ar}/^{39}\text{Ar}$  incremental heating age was determined with a multicollector ARGUS-VI mass spectrometer. After loading the irradiated sample into Cu-planchettes in an ultra-high vacuum sample chamber, it was incrementally heated by scanning a defocused  $\text{CO}_2$  laser beam in preset patterns across the sample, in order to release the Ar evenly. After heating, the reactive gases were cleaned using a SAES Zr-al ST101 getter operated at  $400^\circ\text{C}$ , and two SAES Fe-V-Zr ST172 getters operated at  $200^\circ\text{C}$  and room temperature, respectively. Blank intensities were measured every three incremental heating steps for groundmass. For calculating the ages, the corrected decay constant of Steiger and Jäger (1977) was used:  $5.530 \pm 0.097 \times 10^{-10} \text{ year}^{-1}$  ( $2\sigma$ ) as reported by Min et al. (2000). Incremental heating plateau ages and isochron ages were calculated as weighted means with  $1/\sigma^2$  as weighting factor (Taylor, 1997) and as YORK2 least squares fits with correlated errors (York, 1968) using the ArArCALC v2.7.0 software from Koppers (2002) available online (<http://earthref.org/ArArCALC/website>).

## 4. Results

### 4.1. Description of the Lava Samples

The lavas from Erromango (Figure 1c) were collected from the four old volcanic formations with ages of 5.3 to 1.1 Ma and were described previously (Bellon et al., 1984; Marcelot et al., 1983). Sample 002TVG-1 was recovered by TV-guided grab at 290 m water depth from the top of Vulcan Seamount (Figure 1b) and consists of ankaramitic lava with a 10 cm thick Mn-oxide crust (Table S3). Lava outcrops occur at the steep cliffs of the rifted crust at the SW flank of the horst structure within Vate Trough (Figure 1d) and stratigraphic

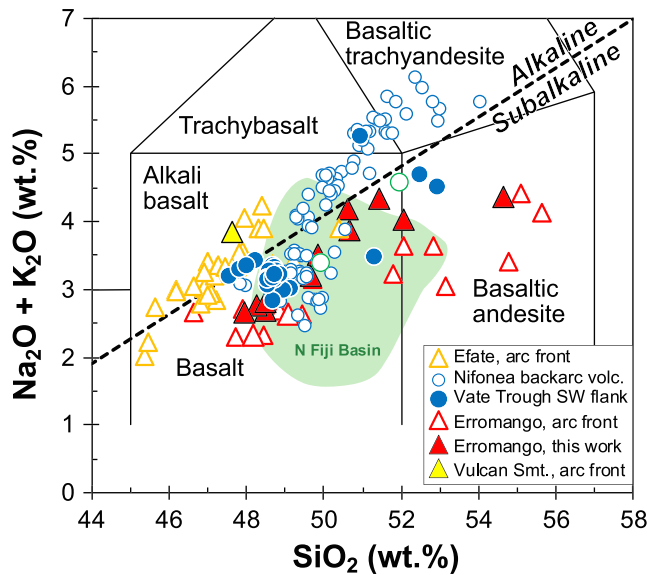


**Figure 3.** Total alkalis-silica (TAS) diagram for the island arc front lavas from Erromango and Vulcan Seamount in comparison to Efate, and of the back-arc lavas from the flank of Vate Trough compared to the recent lavas from the young Nifonea volcano (Lima et al., 2017). Data sources as in Figure 2 and data from the North Fiji Basin (Eissen et al., 1991; Eissen et al., 1994; Nohara et al., 1994).

sampling by ROV between 1,962 to 1,506 m water depth recovered 21 lava samples. The lowermost three samples 072ROV-01 to -03 were collected from talus piles in sediment on the flat base of the cliff. In contrast, the upper samples (072ROV-04 and <1,944 m water depth) were recovered in situ from large outcrops of lava units. The lowermost lava 072ROV-04 yields a groundmass  $^{40}\text{Ar}/^{39}\text{Ar}$  plateau age of  $510.8 \pm 27.3$  kyr. The cliff wall consists of abundant pillow lavas, massive sheet flows, and abundant dykes covered by a thin layer of siliciclastic sediments. Petrographically, the lower part of the profile comprises samples 072ROV-01 to -11, and the upper part corresponds to samples 072ROV-12 to -21.

#### 4.2. Petrography and Mineral Compositions

The lavas from Erromango are mafic and porphyritic containing phenocrysts of olivine, augite, pigeonite, plagioclase, and Ti-magnetite (Marcelot et al., 1983). The ankaramitic lava from Vulcan Seamount contains fresh olivine up to 4 mm in size, green clinopyroxene up to 5 mm, and plagioclase of up to 2 mm. The two lowermost samples from the flank of Vate Trough (072ROV-01 and -02) are intermediate-grained dolerites with an ophitic texture (Table S3) that probably formed in dikes and were not sampled in situ. With the exception of these two samples all other rocks from the Vate Trough flank were recovered from fresh lava flows with little alteration and no Fe- and MnOOH crusts on the surface (Table S3).

Samples 072ROV-08, -15 to -17, -19, and -21 are pillow lavas with a fresh glass rim. All samples above 072ROV-02 are vesicular, fine-grained, and often glassy lavas with rare and small (<2 mm) phenocrysts of olivine and plagioclase (Table S3). The microcrystalline to tachylitic groundmass in the lava samples contains tiny plagioclase laths and sometimes olivine and clinopyroxene crystals.

Plagioclase phenocrysts show sieve texture and pronounced oscillatory zoning in the lower part of the profile (072ROV-02, -06, -08, and -10) with  $\text{An}_{24-91}$  for the core compositions,  $\text{An}_{37-80}$  for the rims and  $\text{An}_{44-81}$  for the groundmass crystals. The samples from the upper part of the profile are more homogeneous with  $\text{An}_{62-81}$  in their cores,  $\text{An}_{75-77}$  in the rims, and  $\text{An}_{61-78}$  for groundmass crystals. Olivine (<30%) crystals are often euhedral and skeletal with normal zoning, but some grains indicate resorption with a rounded shape and embayments. The lower part of the profile has a wide compositional range in olivine phenocrysts with  $\text{Fo}_{74-90}$  ( $n = 87$ ), while the upper part is quite restricted in composition with  $\text{Fo}_{85-89}$  ( $n = 79$ ). The composition of the groundmass crystals is  $\text{Fo}_{76-87}$  ( $n = 33$ ). The more altered samples show partial transformation from olivine to iddingsite. Clinopyroxene phenocrysts are predominantly augite and diopside and occur mainly in the lower lavas (e.g., 072ROV-08, Table S1) but are rare in the upper part of the profile. The composition of phenocryst cores is variable ( $\text{Wo}_{33-44}\text{En}_{34-53}\text{Fs}_{07-23}$ ) ( $n = 71$ ) along the entire profile. Weak zoning is observed in samples 072ROV-06 and -08 with an intragrain Mg# variation of 5% (Mg# = 75–80) and 8% (Mg# = 75–83), respectively. Opaque oxides (e.g., Ti-magnetite) occur in all samples particularly in the matrix, whereas Cr-spinel occurs both as microphenocrysts and inclusions in olivine in the upper lavas.

#### 4.3. Major and Trace Element Composition of the Lavas

In the total alkalis versus  $\text{SiO}_2$  diagram (TAS, Figure 3) most lavas from the arc front volcanoes show distinct compositions where those from Erromango are subalkaline and those from Efate and Vulcan Seamount are transitional. Most lavas from the Vate Trough flank are also subalkaline basalts, but some are transitional basalts, basaltic andesite, and trachybasalt comparable to lavas from Nifonea volcano in the Vate Trough axis (Figures 1 and 3).

In terms of major element composition, the samples from the Vate Trough flank resemble those recovered from the active Nifonea back-arc volcano but differ from those of the arc front. For example, at a given MgO content the lavas recovered on the rift flank of Vate Trough have higher  $\text{TiO}_2$  and  $\text{Na}_2\text{O}$  but lower  $\text{Al}_2\text{O}_3$  than lavas from Efate and Erromango (Figure 4). The  $\text{SiO}_2$  contents of the rift flank lavas are higher for a

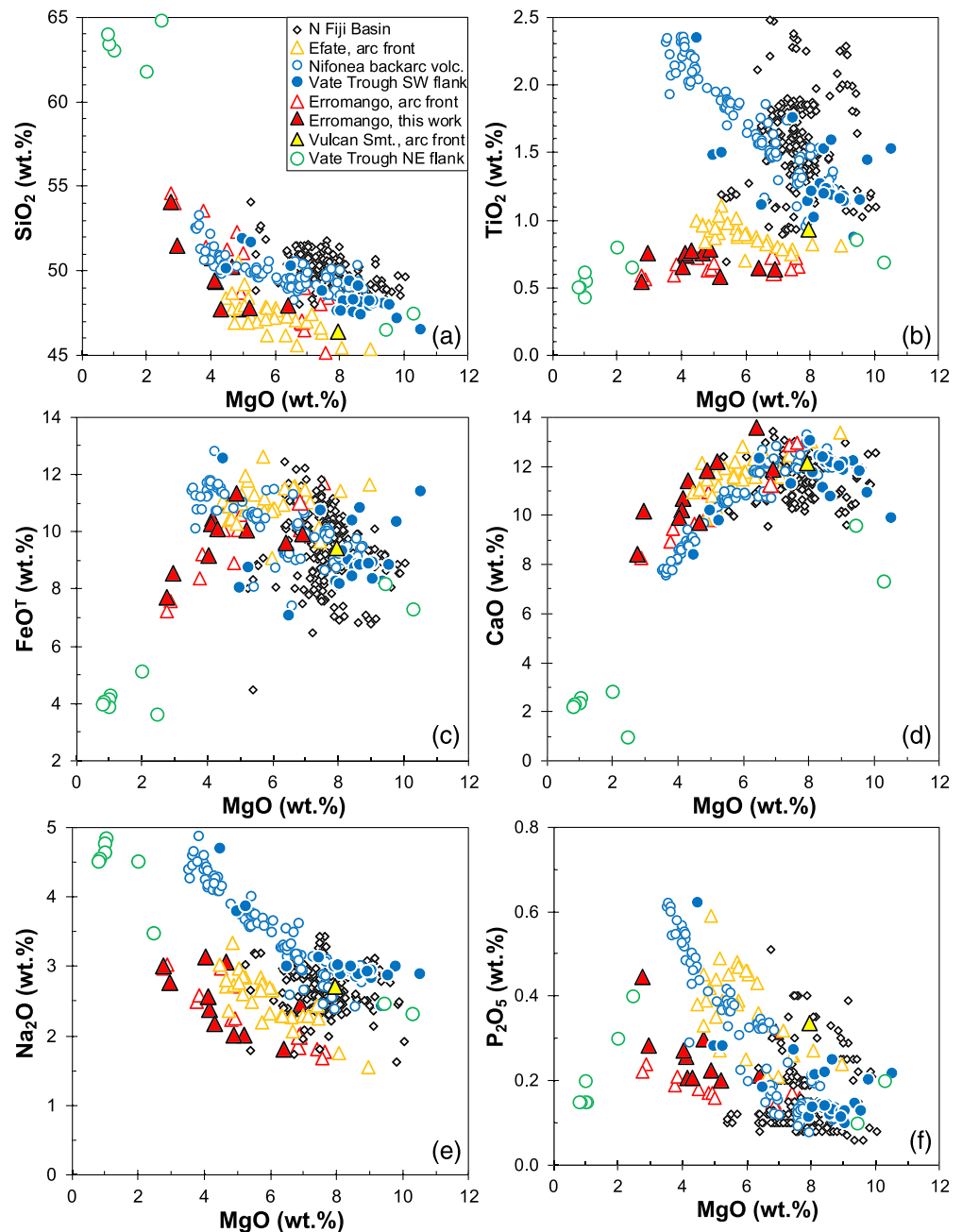


**Figure 4.** Composition of major elements (a) SiO<sub>2</sub>, (b) TiO<sub>2</sub>, (c) FeO<sup>T</sup>, (d) CaO, (e) Na<sub>2</sub>O, and (f) P<sub>2</sub>O<sub>5</sub> versus MgO (wt.%) of the Vate Trough rift flank lavas in comparison to recent lavas from Vate Trough, the arc front volcanoes Erromango, Efate and Vulcan Seamount as well as the older samples recovered from the NE flank of Vate Trough. Data sources as in Figures 2 and 3.

given MgO content than those of the rocks from the island arc front at Efate, Erromango, and Vulcan Seamount, but some lavas from Erromango have similar SiO<sub>2</sub> contents to the back-arc lavas. Volcanic rocks that were recovered on the NE flank of Vate Trough resemble the arc front lavas in major element compositions (e.g., with low TiO<sub>2</sub>), and most lie at the evolved end of the trend of the Erromango lavas (Figure 4).

In contrast to Sr isotope ratios, the incompatible element ratios like Ba/La and Zr/Y do not show a systematic variation along the NHIA or back-arc (Figure 2). The samples from Erromango and sample 002TVG01 from

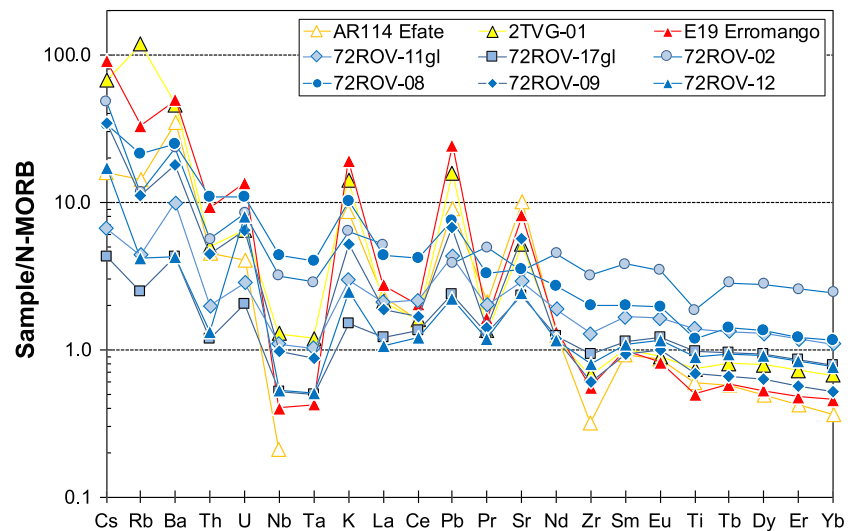


**Figure 5.** N-MORB normalized sample compositions of the basalts from the Vate Trough rift flanks using N-MORB (Sun & McDonough, 1989). Also shown is the pattern of basalt AR114 from Efate in the island arc front (Raos & Crawford, 2004).

Vulcan Seamount in the arc front resemble those from Efate (sample AR114, Raos & Crawford, 2004) in incompatible element ratios and are depleted in Nb, Ta, Zr, and the heavy Rare Earth Elements (REE) but enriched in fluid-mobile elements like Ba, K, and Pb relative to MORB (Figure 5). The back-arc basalts from the Vate Trough flank show a large variation of incompatible element contents, and all basalts are enriched in fluid-mobile elements like Rb, Ba, U, K, and Pb relative to MORB (Figure 5). In contrast, the elements Nb, Ta, Zr, and Ti vary considerably in the Vate Trough flank basalts from being depleted relative to REE in the N-MORB-normalized patterns to Nb-enriched basalts with relatively low MgO contents of 6.5 and 5.5 wt.%.

The Zr/Y and  $(Ce/Yb)_N$  ratios of the lavas broadly increase with decreasing MgO, whereas the other incompatible element ratios, such as Ba/La, remain relatively constant over the range of MgO (Figure 6). At a given MgO content, the Zr/Y of the Erromango and most of the South NHIA lavas are lower than those of the Vate Trough flank and Nifonea basalts (Figure 6a). The Central NHIA lavas show more variation than those from the South NHIA with some, like the Efate basalts, having low Zr/Y, but others overlap with the Nifonea back-arc lavas. The  $(Ce/Yb)_N$  ratios of most of the Erromango and Vulcan Seamount samples are lower than those of Efate but resemble the Nifonea and Vate Trough flank basalts (Figure 6b). On the other hand, all arc front volcanoes resemble each other in Ba/La, whereas the Vate Trough flank lavas have lower Ba/La (Figure 6c). The basalts from the Vate Trough flank are similar to the lavas from the active Nifonea back-arc volcano and North Fiji Basin basalts in terms of their incompatible element ratios. Based on  $(Ce/Yb)_N$  and Zr/Y two groups of lavas can be distinguished in the samples from the Vate Trough flank (Figures 6a and 6b). The majority of the Vate Trough flank lavas have relatively low  $(Ce/Yb)_N$  of ~1, but several samples have higher  $(Ce/Yb)_N$  of ~2 which is similar to the variation observed in the Nifonea volcano.

#### 4.4. Variation of Sr, Nd, and Pb Isotope Ratios in Lavas

Lavas from Erromango generally have higher  $^{87}\text{Sr}/^{86}\text{Sr}$  and lower  $^{143}\text{Nd}/^{144}\text{Nd}$  than basalts recovered at the Vate Trough flank and Nifonea volcano but are lower in Sr and higher in Nd isotope ratios than the volcanic rocks of Efate (Figures 2 and 7a). The basalts with the lowest  $^{87}\text{Sr}/^{86}\text{Sr}$  from the Vate Trough flank and Nifonea volcano overlap with the North Fiji Basin basalts but together with the arc front lavas they trend toward higher Sr at relatively constant Nd isotope ratios (Figure 7a). The Erromango samples have higher  $^{206}\text{Pb}/^{204}\text{Pb}$  than the Efate lavas and those from the Vate Trough flank and Nifonea volcano (Figure 7). The Vulcan Seamount lava sample has a high  $^{87}\text{Sr}/^{86}\text{Sr}$  ratio comparable to the lavas of Efate Island further north (Figure 2a) but higher  $^{206}\text{Pb}/^{204}\text{Pb}$  isotope ratios than Efate rocks. The Vate Trough rift flank lavas cover a range of 18.2 to 18.6 in  $^{206}\text{Pb}/^{204}\text{Pb}$ , which is comparable to that of the recent Nifonea volcano

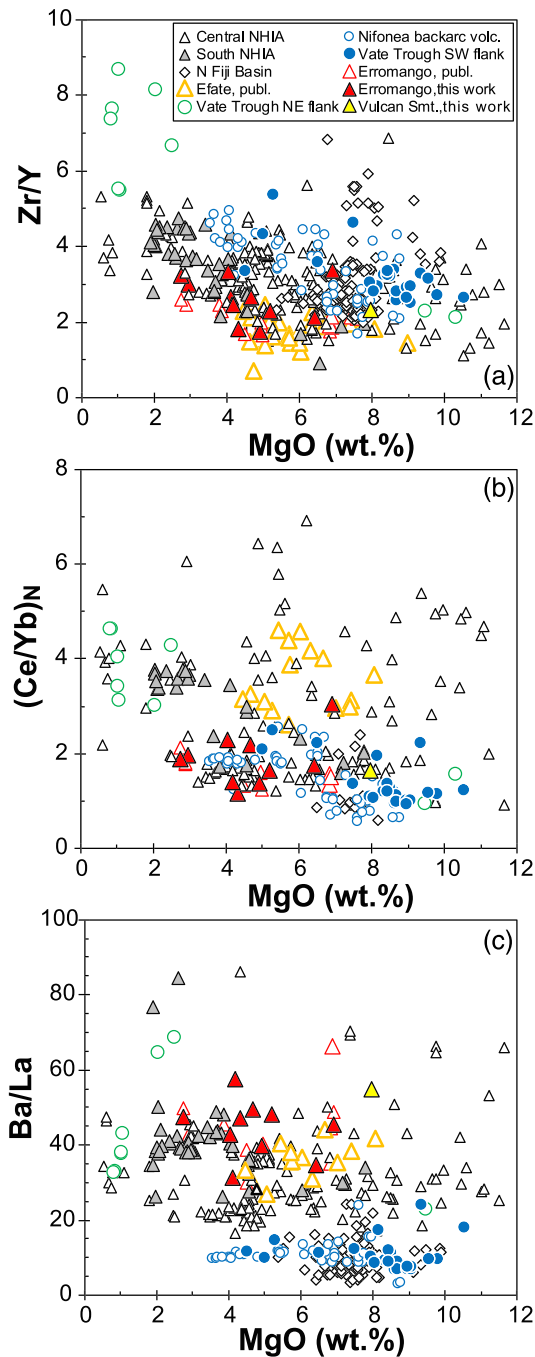


**Figure 6.** Variation of (a) Zr/Y versus MgO, (b)  $(Ce/Yb)_N$  versus MgO, and (c) Ba/La versus MgO comparing the Vate Trough rift flank lavas to the arc front volcanoes Vulcan Seamount, Erromango and Efate and the Nifonea back-arc volcano and older basalts from the Vate Trough flanks. Data sources as in Figures 2 and 3.

basalts (Figure 7b), and both sample groups lie on the Pb isotope trend defined by North Fiji Basin lavas which falls mostly into the field of Indian Ocean MORB (Figure 7b). In contrast, the Erromango lavas form a trend toward higher  $^{206}Pb/^{204}Pb$  but lower  $^{208}Pb/^{204}Pb$  in the field of Pacific Ocean MORB, and the Efate rocks have higher  $^{208}Pb/^{204}Pb$  for a given  $^{206}Pb/^{204}Pb$  compared to the Nifonea volcano basalts. The Sr isotopes of the Vate Trough flank samples are positively correlated with  $^{206}Pb/^{204}Pb$ , similar to the Nifonea basalts (Figure 7c). In contrast, our new Erromango samples and the South NHIA lavas have relatively low  $^{87}Sr/^{86}Sr$  (0.7030–0.7035) for their high  $^{206}Pb/^{204}Pb$ , whereas the Vulcan Seamount sample, lavas from Efate and the other Central NHIA volcanoes have high Sr isotope compositions of  $\sim 0.7040$  and generally low  $^{206}Pb/^{204}Pb$  (Figure 7c). Similarly, the Central and South NHIA lavas form two groups in  $^{143}Nd/^{144}Nd$  versus  $^{206}Pb/^{204}Pb$  (Figure 7d). The Vate Trough flank and Nifonea volcano basalts lie on two trends of relatively constant  $^{143}Nd/^{144}Nd$  but variable  $^{206}Pb/^{204}Pb$ . The South and Central NHIA lavas show variable Ba/La at relatively constant Sr isotope ratios, whereas there is a negative correlation between Nd/Pb and  $^{206}Pb/^{204}Pb$  in the Vate Trough flank and Nifonea volcano basalts (Figures 8a and 8b). All NHIA arc lavas have low Nd/Pb  $\times 10003C$ ; 5 (Figure 8b).

## 5. Discussion

### 5.1. Age and Compositional Variation of the Back-Arc Lavas: Implications for Rifting and Mantle Flow

The horst structure that separates the eastern from the western graben of Vate Trough (Figure 1c) has a seismic signature similar to that of a subaerial arc (McConachy et al., 2005), but the lavas recovered by 072ROV on the Vate Trough flank compositionally resemble the back-arc basalts from the active Nifonea volcano (Figures 4 and 6). Thus, we conclude that the rocks forming the horst structure were formed by back-arc volcanism similar to that at the Nifonea volcano. The uppermost 500 m of lavas of the horst structure at the SW Vate Trough flank are younger than 0.5 Ma, implying that the eastern graben (Figure 1d) formed within a few 100 kyr. Previous dredging (D26 and D27) of the NE rift flanks of Vate Trough (Figure 1d) yielded basaltic to dacitic lavas (Figures 4 and 6) with ages of 3.5 to 2.2 Ma, and at greater depth  $\sim 0.5$  Ma old dacites with an arc signature were recovered (Monjaret et al., 1991). These latter samples appear to be coeval with those recovered from the horst structure further south, but the compositions differ, indicating variable magma formation processes in the Vate Trough. Consequently, back-arc volcanism probably started at  $\sim 0.5$  Ma, although initial rifting may have begun about 2 million years ago (Monjaret et al., 1991).

Both the older Vate Trough flank basalts and those from the active Nifonea volcano have weaker subduction signatures than rocks from the adjacent arc (Figure 5), with low Ba/La values ( $< 25$ ) that resemble the North Fiji Basin lavas and Nd/Pb between 4 and 30 intermediate between MORB and NHIA lavas (Figure 8). Because the Vate Trough back-arc lavas indicate little influence of fluid-mobile elements on their magma formation, they most likely formed by decompression melting of the mantle rather than by flux melting. The variable  $(Ce/Yb)_N$  and isotope ratios in the Vate Trough flank basalts and in the recent Nifonea volcano lavas (Figures 6 and 7) imply

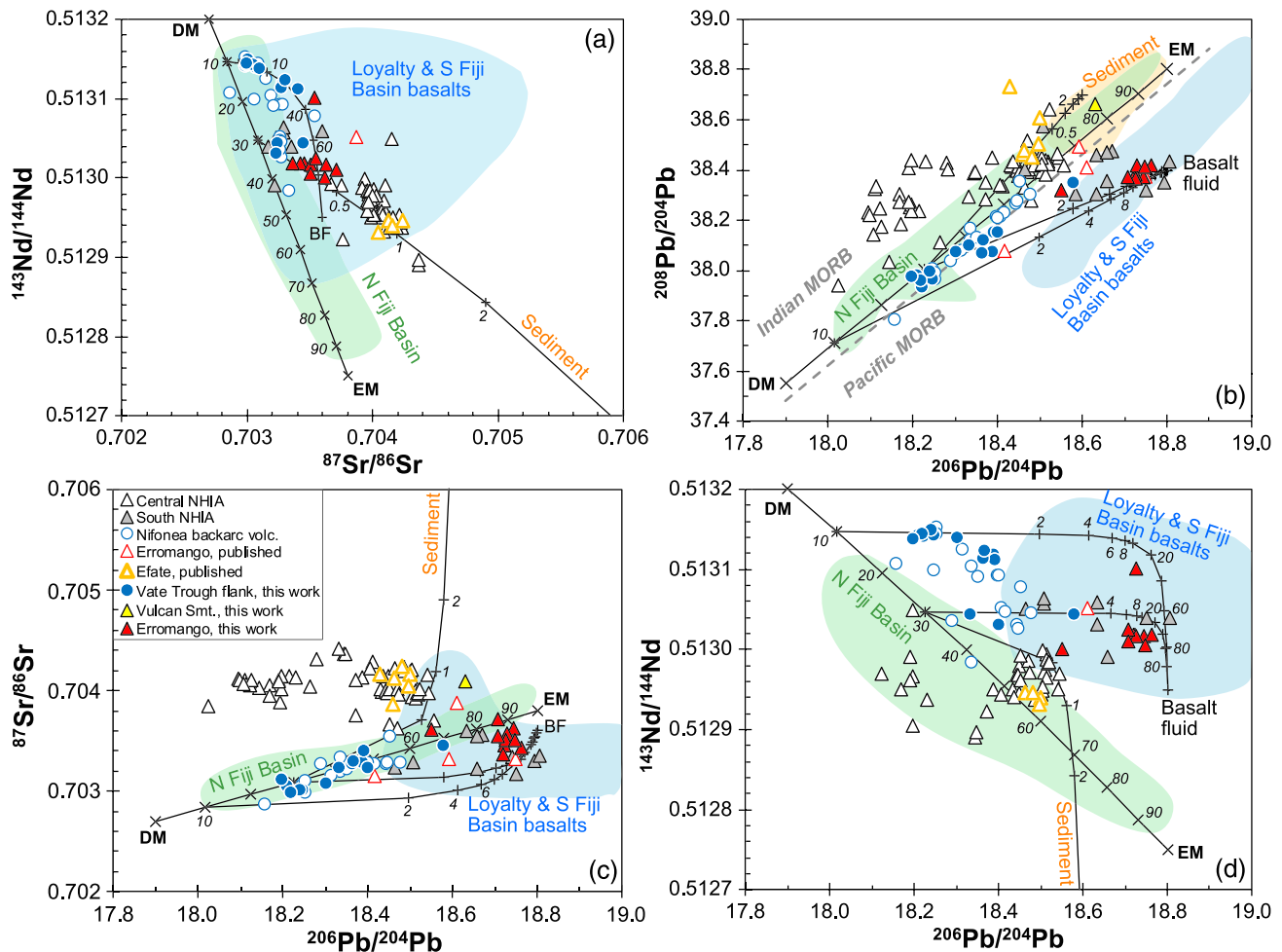


**Figure 7.** (a) Sr versus Nd isotope ratios, (b)  $^{208}\text{Pb}/^{204}\text{Pb}$  versus  $^{206}\text{Pb}/^{204}\text{Pb}$ , (c)  $^{87}\text{Sr}/^{86}\text{Sr}$  versus  $^{206}\text{Pb}/^{204}\text{Pb}$ , and (d)  $^{143}\text{Nd}/^{144}\text{Nd}$  versus  $^{206}\text{Pb}/^{204}\text{Pb}$  of the Vate Trough rift flank lavas compared to the lavas from the arc front volcanoes on Efate and Erromango as well as from the North Fiji Basin and active rift axis of Vate Trough (Heyworth et al., 2011; Kim et al., 2006; Lima et al., 2017; Peate et al., 1997). The compositions of the assumed mixing end-members are provided in Table S4 and discussed in the text. Isotope end-members are estimated from observed variations in the arc and back-arc data as well as from Pacific sediments (Basak et al., 2011; Ben Othman et al., 1989; Peate et al., 1997) and rocks recovered from the subducting crust of the Loyalty (Coltorti et al., 1994; Crawford et al., 1995; Peate et al., 1997) and South Fiji Basins (Mortimer et al., 1998; Todd et al., 2011). The concentrations of Sr and Nd in the sediment melt was taken from an experiment at 800°C by Hermann and Rubatto (2009) and Pb was calculated from the Nd/Pb ratio of the end-member. The depleted and enriched MORB mantle concentrations are from Workman and Hart (2005) and a 5% basalt fluid was calculated using experimental distribution coefficients (Kessel et al., 2005) and altered MORB (Castillo et al., 2009). Other data sources as in Figures 2 and 3. The division line between Pacific and Indian Ocean MORB is after Kempton et al. (2002).

partial melting of mantle sources containing relatively enriched and depleted components resembling those of the North Fiji Basin basalts with little addition by recent subduction. The presence of rift magmas showing little subduction component but varying from depleted tholeiites to enriched alkaline basalts has been observed frequently in early back-arc rifts, for example, in the Sumisu Rift, the Okinawa Trough, and the Tyrrhenian Sea (Hochstaedter et al., 1990; Shinjo et al., 1999; Trua et al., 2010). Additionally, many early back-arc magmas have higher contents of relatively fluid-immobile elements (e.g., higher  $\text{TiO}_2$  and  $\text{Zr}/\text{Y}$ ) than the South NHIA magmas (Figures 2, 4b, and 6a). The depleted mantle signature with  $\text{Zr}/\text{Y} \sim 2$  in mafic lavas ( $\text{MgO} > 5$  wt.%) occurs particularly beneath the South NHIA (Figure 6a), whereas mantle portions yielding basalts with high  $\text{Zr}/\text{Y} > 3$  appear to be restricted to the back-arc and some Central NHIA lavas (Sorbadere et al., 2013), that is, in a region without back-arc troughs. The greater depletion in the South NHIA lavas probably reflects partial melting of the mantle during flow from the back-arc to the arc. The subducting plate causes corner flow of the mantle and thus asthenospheric mantle is flowing from the back-arc into the mantle wedge, which is supported by overlapping compositions in Nd isotopes of the South NHIA

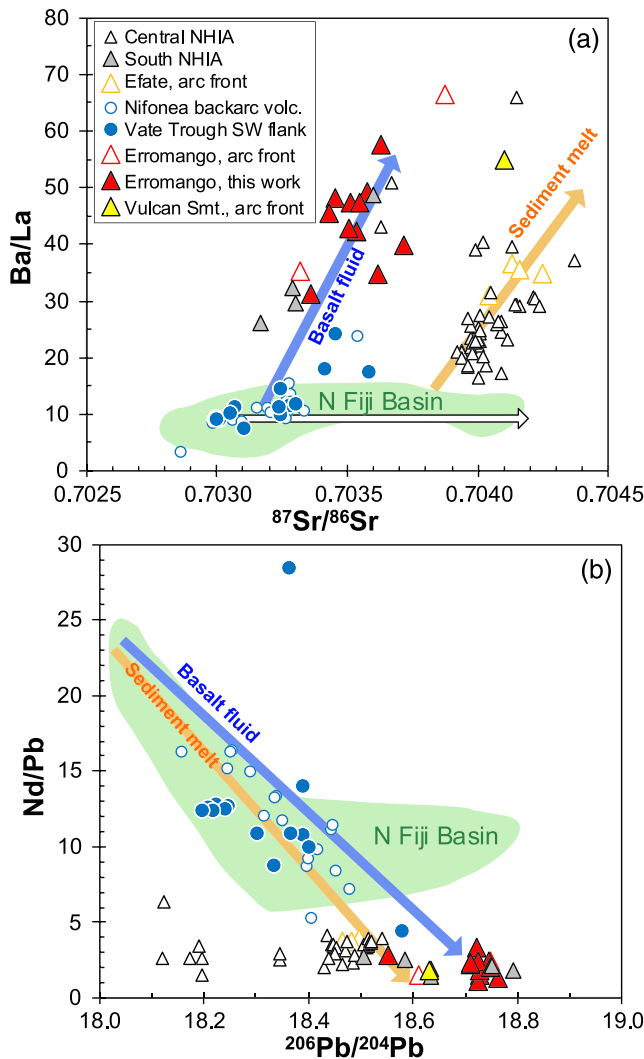


**Figure 8.** (a) Ba/La versus  $^{87}\text{Sr}/^{86}\text{Sr}$ , and (b) Nd/Pb versus  $^{206}\text{Pb}/^{204}\text{Pb}$  of the Vate Trough back-arc lavas compared to those from the arc front volcanoes of Vulcan Seamount, Efate and Erromango, and basalts from the North Fiji Basin. Data sources as in Figures 2 and 3.

and back-arc lavas (Figure 7). In agreement with previous models for other arc/back-arc systems (Hochstaedter et al., 1990; McCulloch & Gamble, 1991; Pearce, 2005; Woodhead et al., 1993), we suggest that the asthenospheric mantle flowing toward the NHIA from the North Fiji Basin is heterogeneous and that the enriched components are removed by partial melting beneath the back-arc troughs. High  $^3\text{He}/^4\text{He}$  isotope ratios of 9.1 R/Ra in hydrothermal fluids from Nifonea volcano (Schmidt et al., 2017) are similar to those of the North Fiji Basin (Ishibashi et al., 1994; Nishio et al., 1998), supporting the inflow of relatively undegassed, lower mantle material from the east. As a consequence, only the more depleted partial melting residue which now has lower Zr/Y, occurs beneath the South NHIA (Figure 6a), whereas many Central NHIA lavas have higher Zr/Y because of the lack of back-arc melting. The high convergence rate of 120 mm/year at the South NHIA (Baillard et al., 2018) probably causes a fast mantle flow that may transport the depleted mantle into the melting region beneath the arc within a few 100,000 years. Models suggest that some 5% depletion of the mantle occurs within 1 million years of back-arc magmatic activity (Hall et al., 2012). Consequently, the inflow of heterogeneous North Fiji Basin mantle, and its melting beneath Vate Trough, means that the mantle delivered to beneath the South NHIA arc front is more depleted in incompatible elements than it would be otherwise.

The cause for rifting in back-arcs is poorly understood and may be driven by motion in either the upper plate (Heuret & Lallemand, 2005) or the subducting slab (Schellart, 2008). Several authors suggested that the lithosphere may be weakened by the hydrous arc magmas which could initiate back-arc rifting (Caratori Tontini et al., 2019; Molnar & Atwater, 1978; Taylor et al., 1991). This model contradicts the observation that early rifting in Vate Trough occurs distant (>30 km) from the New Hebrides arc volcanoes (Figure 1b), which is a situation similar to the Sumisu Rift (Taylor et al., 1991) and the Okinawa Trough (Arai et al., 2017). Additionally, many of the Vate Trough back-arc lavas show a weak geochemical slab component (Ba/La < 15, Nd/Pb > 10, Figure 8) implying that rifting of the back-arc is not caused by flux melting but decompression melting must occur. Recent numerical modeling indicates that the dynamics and temperature of the mantle wedge

may play an important role and active mantle upwelling may cause thinning and rifting of the upper plate (Billen, 2017). Seismic data suggest that the crust is ~28 km thick beneath the New Hebrides arc but may be significantly thinner (perhaps 12 km thick) beneath the Coriolis Troughs (Ibrahim et al., 1980), which would imply significant extension. We suggest that hot mantle containing enriched components flows from the North Fiji Basin into the Vate Trough and partial melting beneath the back-arc for at least the past 0.5 million years is largely due to decompression during the flow, possibly with some contribution by flux melting. Geophysical data suggest that anomalously hot mantle is upwelling beneath the North Fiji Basin (Lagabrielle et al., 1997; Zhang & Pysklywec, 2006) and the lavas erupting along these back-arc spreading centers indicate a heterogeneous source consisting of a range of depleted and enriched components (Figure 7) (Eissen et al., 1994; Nishio et al., 1998). However, Vate Trough appears to be the only one of the three Coriolis back-arc troughs (Figure 1b) with voluminous volcanism (Anderson et al., 2016; Lima et al., 2017; Maillet et al., 1995) supporting the argument that rifting of the lithosphere is not caused by magma intrusion into the lithosphere. At Sumisu Rift, Taylor et al. (1991) observed a similar pattern to the Coriolis Troughs with the back-arc rift basins occurring between the large arc front volcanoes, which they explained by magmatic intrusions that accommodate extension rather than faulting. Thus, normal

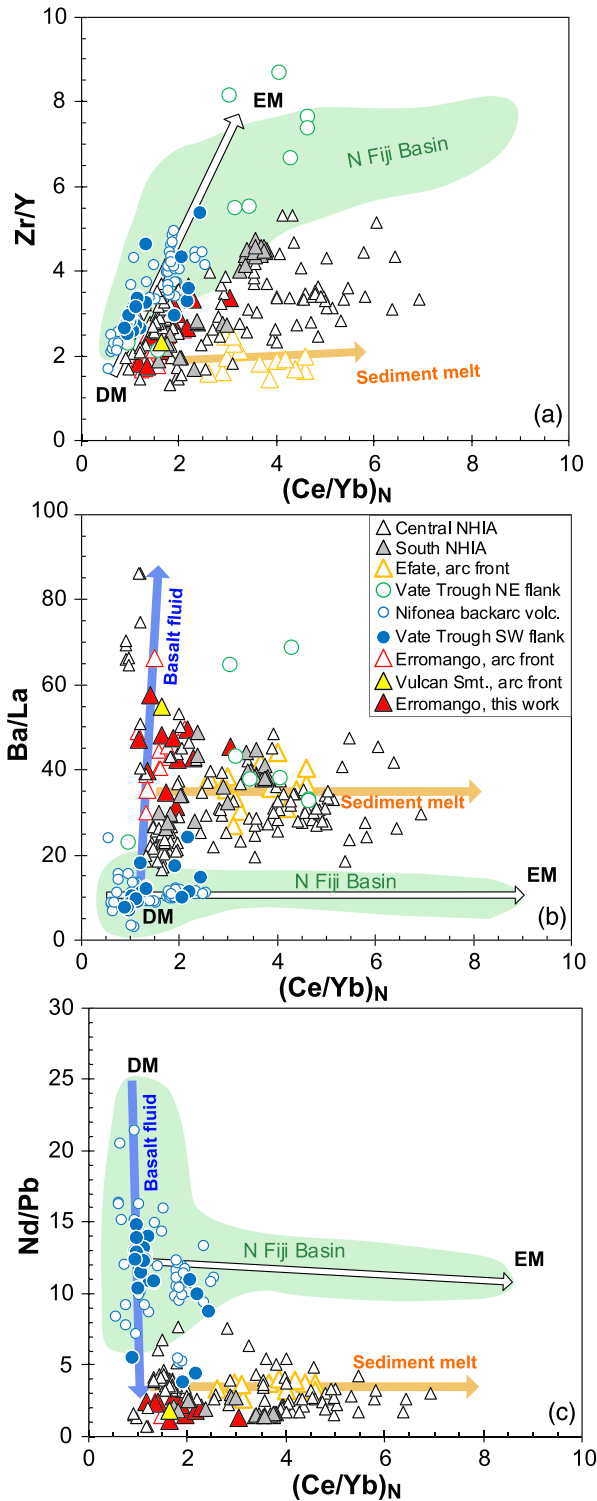


**Figure 9.** (a) Zr/Y versus  $(Ce/Yb)_N$  (b) Ba/La versus  $(Ce/Yb)_N$ , and (c) Nd/Pb versus  $(Ce/Yb)_N$  for the Vate Trough lavas compared to those from the arc front volcanoes of Vulcan Seamount, Efate and Erromango, and basalts from the North Fiji Basin. The mixing processes with the different components discussed in the text are shown as arrows, where the white arrow indicates mixing between depleted (DM) and enriched mantle (EM) sources. Data sources as in Figures 2 and 3.

faulting is probably initiated in the relatively cold crust behind the arc and significant thinning (up to 50%) of the crust occurs within 2 million years, similar to Sumisu Rift (Taylor et al., 1991) and the Coriolis Troughs. We conclude that the arc lithosphere is tectonically rifted behind the arc volcanoes and magma is generated only locally where hot enriched mantle melts adiabatically. We also note that the relatively small Vulcan Seamount in the arc front (Figure 1b) appears to be extinct and the diminished magmatism in the arc front may reflect the fact that lithospheric thinning and partial melting beneath Vate Trough focused magmas into the back-arc.

### 5.2. The Mantle Sources of the Vate Trough Back-Arc Lavas

The incompatible element and radiogenic isotope composition of the Nifonea volcano lavas indicate that they formed by melting of different mantle sources containing (1) a relatively depleted Indian Ocean-type mantle source, (2) an incompatible element-enriched Indian Ocean-type mantle source, and (3) a contribution from the subducting slab (Heyworth et al., 2011; Lima et al., 2017). The data from the older SW Vate Trough flank lavas overlap with those of Nifonea volcano (Figure 7), and thus, the same mantle sources were available for magma formation for the past 0.5 million years. The lavas with the highest Nd/Pb, but the lowest Ba/La have the weakest slab input and have the lowest Sr and Pb isotope ratios (Figure 8). For example, the correlation between Nd/Pb and  $^{206}Pb/^{204}Pb$  isotope ratios suggests a depleted MORB-like end-member with a  $^{206}Pb/^{204}Pb$  of 17.9 to 18.1 similar to some lavas from the North Fiji Basin (Figure 8b). Similarly, the samples from the Vate Trough flank with Ba/La  $\times 0003C$ ; 10 have  $^{87}Sr/^{86}Sr$  of  $\sim 0.7030$  similar to the depleted end-member observed in the North Fiji Basin basalts (Figure 8a). The Vate Trough flank basalts with the low  $^{206}Pb/^{204}Pb$  have relatively high  $^{208}Pb/^{204}Pb$  and lie within the field of Indian Ocean-type MORB but close to the boundary defined by Kempton et al. (2002) in agreement with previous work on the Vate Trough basalts (Heyworth et al., 2011; Lima et al., 2017). Consequently, the Indian Ocean MORB-type end-member has been present beneath the Vate Trough for at least 0.5 Ma.

Most Vate Trough flank lavas have higher  $^{87}Sr/^{86}Sr$  and  $^{206}Pb/^{204}Pb$  isotope ratios for a given Nd isotope ratio than those of the North Fiji Basin basalts, but those with the lowest Sr and Pb isotope ratios resemble the North Fiji Basin basalts (Figure 7). The incompatible element ratios  $(Ce/Yb)_N$ , Zr/Y, and Ba/La also suggest similarities between the North Fiji Basin mantle and those of the Vate Trough flank (Figure 9). Thus, the Nd isotope, Ba/La and  $(Ce/Yb)_N$  variations largely reflect the heterogeneous mantle wedge prior to the addition of a slab component, which is also observed in some Central NHIA lavas (Sorbadere et al., 2013). As noted above, most of the Vate Trough flank basalts lie close to the boundary but in the field of Indian Ocean MORB (Figure 7b), but those with higher Pb isotope compositions trend into the field of Pacific MORB and toward the composition of the Erromango lavas (Figure 7b). The trends in Figures 7a and 7d suggest that variable mantle wedge material with  $^{143}Nd/^{144}Nd$  of  $\sim 0.51315$  and  $\sim 0.51305$  is mixing with the subduction component affecting Erromango and other South NHIA magmas.

Similar effects of a slab component on the Vate Trough flank basalts are observed in the samples with the highest Ba/La and lowest Nd/Pb (Figure 9). We conclude that the Sr and Pb isotope composition of the Vate Trough flank lavas reflects the influence of this slab component on the heterogeneous Indian Ocean-type back-arc mantle.

### 5.3. The Composition of the Mantle Wedge Beneath the NHIA

Several authors noted the difference in isotopic composition between lavas from the Central NHIA, including Efate and those further south and north (Briqueu et al., 1994; Crawford et al., 1995; Peate et al., 1997). Whereas the Central NHIA volcanoes formed from a source with  $^{87}\text{Sr}/^{86}\text{Sr} > 0.7036$  and  $^{206}\text{Pb}/^{204}\text{Pb} < 18.6$ , lavas from the southern volcanoes have  $^{87}\text{Sr}/^{86}\text{Sr} < 0.7036$  and  $^{206}\text{Pb}/^{204}\text{Pb} > 18.6$  (Briqueu et al., 1994; Crawford et al., 1995; Laporte et al., 1998; Peate et al., 1997). Our new data from Vulcan Seamount in the New Hebrides arc front indicate that the boundary between the two mantle domains occurs between Erromango and Vulcan Seamount at  $\sim 18.5^\circ\text{S}$  (Figures 1b and 2). The Central NHIA signature in Vulcan Seamount implies that the collision of the D'Entrecasteaux Ridge had an effect on magmatism further south than previously assumed, that is, the geochemical effect on the arc is some 50 km wider than in earlier estimates.

The composition of the Central NHIA volcanoes apparently changed from the Pacific MORB-type signature to that of Indian MORB between 2 and 1.5 Ma ago when the arc collided with the D'Entrecasteaux Ridge (Briqueu et al., 1994). Different mantle sources with Indian MORB-type mantle beneath the Central NHIA volcanoes and Pacific MORB-type mantle beneath those of the South NHIA were suggested previously (Crawford et al., 1995). The difference was defined on the basis of  $^{208}\text{Pb}/^{204}\text{Pb}$  versus  $^{206}\text{Pb}/^{204}\text{Pb}$  (Figure 7b) where Indian and Pacific MORB show distinct compositions (Briqueu et al., 1994; Crawford et al., 1995; Laporte et al., 1998; Peate et al., 1997). However, both Sr and Pb isotopes show correlations with Ba/La and Nd/Pb, respectively, that imply effects of slab components on the isotope composition (Figure 8). For example, both the low and the high  $^{206}\text{Pb}/^{204}\text{Pb}$  components in the NHIA lavas are associated with low Nd/Pb of 1 to 3 (Figure 8b) compared with  $\sim 25$  in midocean ridge basalt (MORB) (Hofmann, 2003). Lead is more fluid-mobile than Nd (Brenan et al., 1995) and sediments have Nd/Pb  $\sim 0.003$ ; 3 (Peate et al., 1997) implying that the magmas of Efate, Vulcan Seamount, Erromango, and other NHIA volcanoes are enriched in Pb by a subduction component with a  $^{206}\text{Pb}/^{204}\text{Pb}$  composition that varies from 18.1 to 18.8 (Figures 5 and 8b). This addition causes the deviation of the Pb (and Sr) isotope trends at a given  $^{143}\text{Nd}/^{144}\text{Nd}$  of the NHIA lavas from that of the North Fiji Basin basalts (Figures 7a and 7d). Consequently, in contrast to previous work (Briqueu et al., 1994; Crawford et al., 1995; Laporte et al., 1998; Peate et al., 1997), we suggest that the different Pb and Sr isotopic compositions of the NHIA lavas reflect input from the subducting slab rather than the mantle source. Thus, although the mantle beneath the Central NHIA and the Vate Trough has a composition resembling the back-arc basalts (Heyworth et al., 2011; Lima et al., 2017), which in turn has a composition similar to Indian Ocean MORB as indicated by Nd and Hf isotopes (Pearce et al., 2007), the Pb isotope composition rather reflects the slab component.

South of  $18.5^\circ\text{S}$  the subducting plate apparently releases a component with low Sr and high Pb isotope composition resembling Pacific MORB (Figure 7b). Based on the Nd and Hf isotope data, Pearce et al. (2007) found that South NHIA lavas from Erromango and Tanna fall into the field of Indian MORB. Sediment addition to a Pacific MORB source may have caused a shift of the composition of the mantle (Pearce et al., 2007). Alternatively, the mantle beneath parts of the South NHIA may also be Indian Ocean MORB-type similar to the associated Vate Trough back-arc basalts. The two samples defining the high  $^{230}\text{Th}/^{232}\text{Th}$  of Pacific Ocean mantle are from Matthew island, that is, the southernmost NHIA at  $22.3^\circ\text{S}$  (Turner et al., 1999) and could indicate that Pacific Ocean-type mantle occurs only in the southernmost NHIA. Although the composition of the mantle wedge beneath the South NHIA remains ambiguous, the Pacific Ocean-type signature in Pb isotopes likely reflects a slab component.

### 5.4. The Slab Components Affecting the New Hebrides Island Arc Magmas

Peate et al. (1997) proposed relatively constant addition of 1% to 3% bulk sediment to the mantle wedge of the NHIA where most of the variation in  $^{143}\text{Nd}/^{144}\text{Nd}$  reflects the differences between Indian and Pacific Ocean-type mantle beneath the Central and South NHIA, respectively. The composition of lavas from the Central NHIA volcanoes Lopevi, Efate, and Epi indicate a contribution of sediment fluids and melts to

the mantle wedge (Beaumais et al., 2013; Beier et al., 2018; Raos & Crawford, 2004). The variations of incompatible element ratios with Sr and Pb isotope compositions (Figure 8) suggest different slab components, with that of the South NHIA having low  $^{87}\text{Sr}/^{86}\text{Sr}$  and high  $^{206}\text{Pb}/^{204}\text{Pb}$  whereas that of the Central NHIA has high  $^{87}\text{Sr}/^{86}\text{Sr}$  and low  $^{206}\text{Pb}/^{204}\text{Pb}$ . The slab component with  $^{206}\text{Pb}/^{204}\text{Pb} < 18.5$  observed in the Central NHIA lavas is interpreted as a mixture of basalt-derived fluids and sediments (Sorbadere et al., 2013). The crust of the North Loyalty and South Fiji Basins that is subducted beneath the NHIA has ages between 28 and 46 Ma and the D'Entrecasteaux Ridge consists of Eocene arc tholeiites (Coltorti et al., 1994; Mortimer et al., 2014; Sdrolias et al., 2003). About 650 m of volcanoclastic and carbonate sediments were drilled above basalt and gabbro at DSDP Leg 30 Site 286 in the North Loyalty Basin west of the Central NHIA (Packham & Andrews, 1975). The analyzed volcanoclastic sediments have  $^{206}\text{Pb}/^{204}\text{Pb}$  in the range 18.5 to 18.8 (Peate et al., 1997), whereas basalts from the D'Entrecasteaux Ridge have  $^{206}\text{Pb}/^{204}\text{Pb}$  of 18.5 to 18.6, and one sample has a significantly higher ratio of 19.36 (Coltorti et al., 1994; Peate et al., 1997). Little is known about sediments and oceanic crust of the North Loyalty and South Fiji Basins south of Site 286, but dredged basement samples range from back-arc basalt to intraplate basalt and rhyolite with variable isotopic compositions (Figure 7) and  $^{206}\text{Pb}/^{204}\text{Pb}$  up to 19.5 (Mortimer et al., 1998; Mortimer et al., 2007; Mortimer et al., 2014; Todd et al., 2011). The slab end-member of Central NHIA lavas like those from Efate and Vulcan Seamount has  $\text{Ba}/\text{La} > 30$ ,  $\text{Nd}/\text{Pb} \sim 0.003$ ; 3,  $^{87}\text{Sr}/^{86}\text{Sr} > 0.704$ ,  $^{206}\text{Pb}/^{204}\text{Pb}$  of 18.5 to 18.6, and  $^{208}\text{Pb}/^{204}\text{Pb} > 38.6$  (Figures 7 and 8). High  $^{208}\text{Pb}/^{204}\text{Pb}$  values are typical for pelagic sediments (Figure 7), and thus, we agree with Peate et al. (1997) that this slab component was released from subducting sediments. Compared to the North Fiji Basin basalts, the Central NHIA lavas have high  $(\text{Ce}/\text{Yb})_{\text{N}}$  for a given  $\text{Zr}/\text{Y}$  but low Nb contents (Figures 5 and 9). Consequently, the high  $(\text{Ce}/\text{Yb})_{\text{N}}$  values do not reflect mixing with an incompatible element-enriched mantle source but rather the slab component which is Nb-depleted because of residual rutile and/or relatively low Nb contents in sediments (Hermann & Rubatto, 2009).

It has been shown by experimental work that variable temperature in subducting sediments causes formation of either hydrous fluids or melts that show a variable fractionation between incompatible elements (Hermann & Rubatto, 2009; Spandler et al., 2007). Experimentally determined fluids from sediments have high  $\text{Ba}/\text{La}$  but low  $(\text{Ce}/\text{Yb})_{\text{N}}$ , whereas melts from sediments have low  $\text{Ba}/\text{La}$  but high  $(\text{Ce}/\text{Yb})_{\text{N}}$  (Hermann & Rubatto, 2009; Spandler et al., 2007). In the model in Figure 7 we use the concentrations of Sr and Nd of 259 ppm and 12 ppm (Table S4), respectively, found in sediment melts at 800°C at 3.5 GPa (Hermann & Rubatto, 2009). The sediment used in this experiment has very high Pb contents of 213 ppm (Hermann & Rubatto, 2009) causing extreme Pb contents in the melts. In contrast, Pacific Ocean pelagic clay has Pb concentrations <60 ppm (Ben Othman et al., 1989), and we estimate the Pb content from the low  $\text{Nd}/\text{Pb}$  of the sediment end-member in Figure 8b to have possibly 15 ppm Pb. Mixing calculations with the isotope compositions shown in Table S4 and the concentrations of the sediment melt as well as depleted and enriched MORB (Workman & Hart, 2005) yield results of <1% addition of a sediment melt to the variably depleted mantle to explain the Efate lava compositions (Figure 7). Thus, we suggest that the low  $\text{Ba}/\text{La}$  and high  $(\text{Ce}/\text{Yb})_{\text{N}}$  of the Vulcan Seamount, Efate, and Central NHIA lavas indicate mixing of small amounts of partial melts from subducted sediments into the mantle wedge. The D'Entrecasteaux Ridge collision with the Central NHIA forms an accretionary wedge (Greene et al., 1994) and subduction of the ridge may cause increased sediment recycling.

In contrast, the Erromango and South NHIA lavas require a slab component with  $^{206}\text{Pb}/^{204}\text{Pb} \sim 18.8$  and  $^{208}\text{Pb}/^{204}\text{Pb} \sim 38.4$  but low  $^{87}\text{Sr}/^{86}\text{Sr}$  of  $\sim 0.7036$ , which is unlikely to be caused by pelagic sediment (Figure 7). The relatively high  $\text{Ba}/\text{La} > 50$  and low  $\text{Nd}/\text{Pb}$  and  $(\text{Ce}/\text{Yb})_{\text{N}}$  affecting Erromango magmas could be a hydrous fluid from altered basalt but the mafic rocks drilled at Site 286 have  $^{206}\text{Pb}/^{204}\text{Pb}$  of 18.2 to 18.5, that is, too low to represent this slab end-member. We note, however, that the volcanic rocks of the North Loyalty and South Fiji Basins fall into the field of Pacific MORB (Figure 7b), and if rocks with more radiogenic Pb occur on this plate, they may cause the Pacific-type signature in the southern New Hebrides lavas. Alkaline basalts occur on seamounts of the Loyalty Ridge (Mortimer et al., 2018) and rocks with radiogenic Pb (e.g.,  $^{206}\text{Pb}/^{204}\text{Pb} > 19.0$ ) were recovered from the South Fiji and Norfolk Basins (Mortimer et al., 1998; Todd et al., 2011). Thus, we speculate that the altered basaltic crust of the North Loyalty and South Fiji Basins represents the Pacific MORB-type subduction component of Erromango (Figure 7) and possibly all southern New Hebrides arc magmas but that rocks representing this end-member have not been drilled at Site 286. The Erromango and Vulcan Seamount lavas require an end-member with high  $\text{Ba}/\text{La} > 50$  but

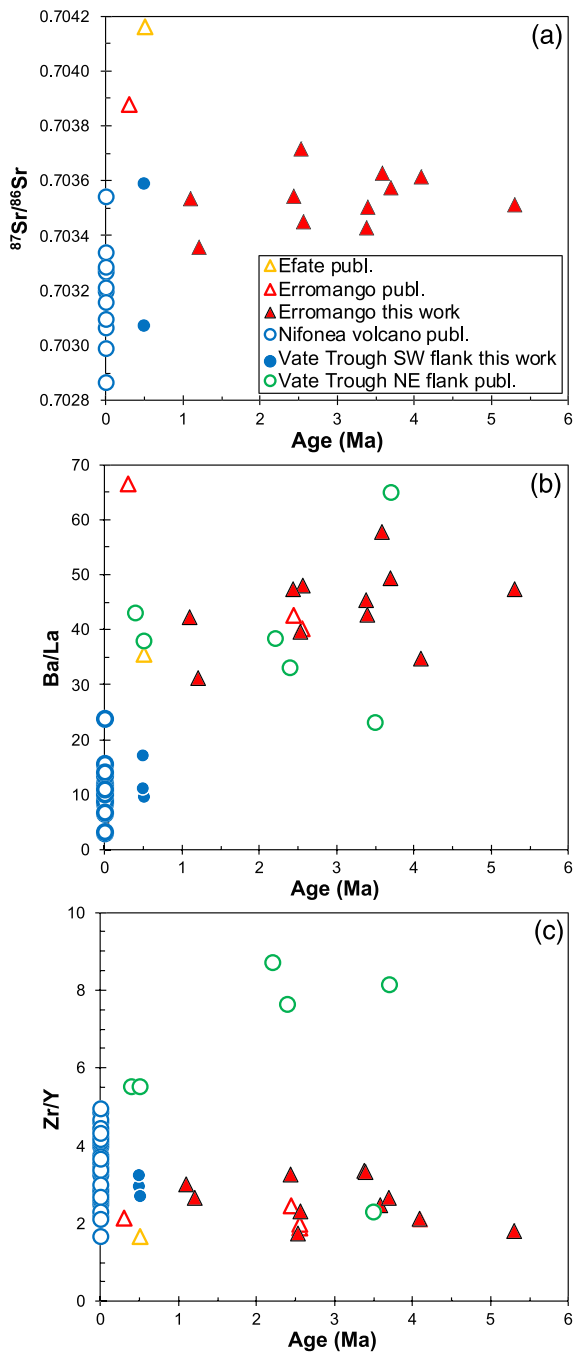


**Figure 10.** Variation of (a)  $^{87}\text{Sr}/^{86}\text{Sr}$ , (b) Ba/La, and (c) Zr/Y versus age showing no variation in the composition of Erromango lavas in the past 5 million years. Age data are from Bellon et al. (1984) and samples from the NE flank of Vate Trough from Maillet et al. (1995) and Monjaret et al. (1991).

low  $(\text{Ce}/\text{Yb})_N < 2$  (Figure 9b), and we suggest that this represents a hydrous fluid from subducted altered basalt (Kessel et al., 2005), as indicated by the relatively low Sr and high Pb isotopes (Figures 7 and 8). We calculate the composition of a 5% hydrous fluid using altered MORB composition (Castillo et al., 2009) and distribution coefficients at 700°C (Kessel et al., 2005) which yields 51.7 ppm Sr, 0.39 ppm Nd, and 1.4 ppm Pb (Table S4). With these concentrations and previously defined isotope ratios of the altered basalt we find the mixing curves with variably depleted MORB mantle (Workman & Hart, 2005). The model suggests that the Sr, Nd, and Pb isotope composition of the Erromango lavas largely (>60%) reflect the hydrous fluid released from the slab (Figure 7).

### 5.5. The Slab Components in the Vate Back-Arc Magmas

The enrichment of fluid-mobile elements in some of the basalts from the Vate Trough rift flank and Nifonea volcano (Figures 9b and 9c) indicates a contribution from the subducting slab to the melts since 0.5 Ma. Lima et al. (2017) suggested that the active Nifonea volcano magmas are affected by a sediment component, which is supported by the Pb isotope ratios trending toward the Central NHIA compositions (Figure 7b). However, many elements, including Nd, are little or not affected by the slab component and reflect compositional variation of the back-arc mantle. For example, at relatively constant Nd isotope ratios, Sr and Pb isotope compositions show significant deviations from North Fiji Basin basalts (Figure 7). These variations in  $^{87}\text{Sr}/^{86}\text{Sr}$  and  $^{206}\text{Pb}/^{204}\text{Pb}$  correlate with enrichment of fluid-mobile elements indicated by Ba/La and Nd/Pb (Figure 8). Most of the variation in isotope compositions of the Vate Trough flank basalts with relatively low  $^{87}\text{Sr}/^{86}\text{Sr}$  and  $^{208}\text{Pb}/^{204}\text{Pb}$  can be explained by the influence of a fluid from altered Loyalty Basin basalts similar to that affecting Erromango (Figure 7). However, the mixing curves in Figure 7 suggest <20% addition of basaltic fluid for Sr and Nd, whereas the Pb isotopes require only <2% addition of the fluid affecting Erromango mantle. This difference possibly indicates that the fluid affecting the Vate Trough flank basalt source had a slightly different composition than the model fluid. The trend in Pb isotopes of the Vate Trough flank lavas appears to differ from that of the Nifonea Volcano basalts (Figure 7b) and more radiogenic Vate Trough flank basalts have compositions in the field of Pacific Ocean-type lavas with the sample with highest Pb isotopes resembling South NHIA lavas (Figure 7). This slight change of the slab end-member may indicate that the slab component affecting the back-arc magmas changes with time. We speculate that the older melts represented by the Vate Trough flank rocks contained a fluid from subducted altered basalt, whereas the young Nifonea lavas indicate an increasing input of a sediment component.

The slab at the Vanuatu trench dips very steeply and, although the slab beneath the Vate Trough (~220 km distant from the trench) lies at a depth of ~300 km (Hayes et al., 2012), a fluid signal can be observed in the Vate Trough lavas (Lima et al., 2017). Estimates of the water release from the slab suggest significant dehydration to this depth (van Keken et al., 2011; Wilson et al., 2014), but a lateral transport of fluid-metasomatized mantle from the shallow slab to the back-arc melting zone is also possible (Gerya, 2011). The steep slab dip of 67° to 70° at the New Hebrides subduction zone (Syracuse & Abers, 2006) causes most water release over a small region, a narrow melting zone, and relatively low

melt production beneath the arc (Cagnioncle et al., 2007). On the other hand, water release at deeper levels, as well as the ascent of this water to the shallow mantle, has been modeled (Wilson et al., 2014) and may apply to the Vate Trough back-arc. Volcanic activity in Vate Trough is restricted to Nifonea volcano in the back-arc behind Vulcan Seamount and it appears that the slab-influenced Vate Trough lavas lie on mixing curves with the Vulcan composition (Figures 7, 8, and 9) whereas the older Vate Trough flank lavas may be affected by a component similar to that of Erromango magmas. Thus, we suggest that the sediment component affecting Vulcan Seamount magmas is also transported into the melting zone beneath the Vate Trough back-arc.

### 5.6. The Magmatic Evolution of the Arc Front Volcanoes

The Erromango volcanoes have been active since about 5 Ma (Bellon et al., 1984) which allows us to determine whether there was any change in subduction input over this period. However, both Sr isotope ratios and Ba/La remain constant (Figures 10a and 10b), implying that the subducting slab released relatively constant fluids in the past 5 million years. Thus, although the collision of the D'Entrecasteaux Ridge further north caused a change in Sr isotope composition from 0.7029 to 0.7040 in the volcanic rocks of the Aoba Basin (Briqueu et al., 1994; Crawford et al., 1995), there is no effect observed in the lavas erupted south of the collision. We conclude that only the region north of 18°S was affected by the subduction of the D'Entrecasteaux Ridge, which largely coincides with the area with relatively few earthquakes (Baillard et al., 2018).

Many island arc/back-arc systems show an extreme depletion of the arc front magmas in terms of Nb and Zr contents that has been explained by partial melting of the mantle beneath the back-arc before flowing to the arc front (McCulloch & Gamble, 1991; Woodhead et al., 1993). The variation of the Zr/Y and (Ce/Yb)<sub>N</sub> ratios of the Vate Trough flank lavas is comparable to that of Nifonea back-arc basalts, and the North Fiji Basin basalts (Figures 6 and 9). Thus, the mantle beneath the Vate Trough contains variably depleted components that mix during partial melting in different proportions. In contrast, the mantle beneath the South NHIA front appears to be comparable to the most depleted back-arc lavas having, for example, among the lowest Zr/Y (Figures 6b and 9a). Interestingly, the arc lavas from Erromango show a similar Zr/Y composition for the past 5 Ma (Figure 10c), although melting in the back-arc occurred only since ~0.5 Ma. Thus, there appears to be no change toward more residual compositions after onset of melting in the back-arc. This suggests that the evolution of the NHIA back-arc with increasing extension and potentially increasingly larger magma volumes does not cause increasing depletion of the mantle wedge beneath the arc front volcanoes. Consequently, either the mantle flowing beneath Erromango prior to 0.5 Ma did not contain enriched components, or these components became diluted by the large degrees of partial melting beneath the arc.

The volcanism of Erromango, as well as that of other New Hebrides arc front volcanoes, seems to migrate away from the trench, because the youngest volcanoes lie east of the older volcanoes on the islands (Figure 1b). Such a migration may reflect either erosion of the upper plate or the shallowing of the slab (Jicha & Kay, 2018). The subduction of the D'Entrecasteaux Ridge appears to cause upper plate erosion in the Central NHIA (Greene et al., 1994) but cannot explain the eastward migration of volcanism at Erromango and Tanna. Thus, we suggest that the migration of volcanism at the South NHIA is due to a shallowing of the dip angle of the slab in the past 5 million years. This may be caused by the flow of mantle toward the trench and the retreating slab (Heuret & Lallemand, 2005). Thus, the lateral flow of hot asthenospheric mantle may not only lead to the formation of back-arc rifting and magma formation due to adiabatic melting of enriched portions, but also to arc migration.

## 6. Conclusions

The basalts sampled along the 500 m high profile at the SW Vate Rift flank represent a <0.5 Ma-old succession of lavas erupted during the early rifting of the Vate Trough. The magmas formed by decompression melting from a mantle that is heterogeneous on a small scale containing variably depleted portions which is likely flowing in from the North Fiji Basin. This mantle was fluxed initially by hydrous fluids from subducting altered basalts, whereas recent back-arc magmas indicate a slab component from sediments similar to the arc front volcano of Vulcan Seamount. Rifting and tectonic faulting preceded local partial melting of hot material flowing into the mantle wedge beneath Vate Trough, implying that the magmas probably played no active role in the rifting process. Magma formation in the back-arc regions appears to be

restricted to regions where enriched fusible mantle is concentrated. The enriched material is efficiently depleted in the back-arc and does not occur beneath the South NHIA front. The slab component varies from hydrous melts from subducted sediments in the Central NHIA to fluids from altered basalts in the South NHIA. This basaltic fluid has affected the South NHIA for at least 5 million years without apparent changes, whereas there was a significant change in slab component in the Central NHIA due to the collision of the D'Entrecasteaux Ridge.

### Data Availability Statement

All data used in this manuscript are found in Tables S1 to S4, and geochemical data are available in the PANGAEA data repository (<https://doi.org/10.1594/PANGAEA.922017>).

### Acknowledgments

We gratefully acknowledge the help of Captain D. Korte, his crew of RV Sonne, and the ROV Kiel 6000 crew during sample recovery and the entire SO229 scientific party for a successful and pleasant cruise. We thank R. Arculus, T. Tevi, H. Cook, and T. McConachy for their help in organizing the cruise, and D. Miggins and A. Koppers for Ar/Ar age dating. Constructive reviews by P. Kempton, D. Peate, and J. Ribeiro significantly improved the quality of this work. This project 03G 0229 was funded by the German Bundesministerium für Bildung und Forschung (BMBF).

### References

- Anderson, M. O., Hannington, M. D., Haase, K., Schwarz-Schampera, U., Augustin, N., McConachy, T. F., & Allen, K. (2016). Tectonic focusing of voluminous basaltic eruptions in magma-deficient backarc rifts. *Earth and Planetary Science Letters*, *440*, 43–55. <https://doi.org/10.1016/j.epsl.2016.02.002>
- Arai, R., Kodaira, S., Yuka, K., Takahashi, T., Miura, S., & Kaneda, Y. (2017). Crustal structure of the southern Okinawa Trough: Symmetrical rifting, submarine volcano, and potential mantle accretion in the continental back-arc basin. *Journal of Geophysical Research*, *122*, 622–641. <https://doi.org/10.1002/2016JB013448>
- Baillard, C., Crawford, W. C., Ballu, V., Pelletier, B., & Garaebiti, E. (2018). Tracking subducted ridges through intermediate-depth seismicity in the Vanuatu subduction zone. *Geology*, *46*(9), 767–770. <https://doi.org/10.1130/G45010.1>
- Baillard, C., Crawford, W. C., Ballu, V., Régner, M., Pelletier, B., & Garaebiti, E. (2015). Seismicity and shallow slab geometry in the central Vanuatu subduction zone. *Journal of Geophysical Research*, *120*, 5606–5623. <https://doi.org/10.1002/2014JB011853>
- Barsdell, M., & Berry, R. F. (1990). Origin and evolution of primitive island arc ankaramites from Western Epi, Vanuatu. *Journal of Petrology*, *31*(3), 747–777. <https://doi.org/10.1093/petrology/31.3.747>
- Barsdell, M., Smith, I. E. M., & Spörl, K. B. (1982). The origin of reversed geochemical zoning in the northern New Hebrides volcanic arc. *Contributions to Mineralogy and Petrology*, *81*(2), 148–155. <https://doi.org/10.1007/BF00372051>
- Basak, C., Martin, E. E., & Kamenov, G. D. (2011). Seawater Pb isotopes extracted from Cenozoic marine sediments. *Chemical Geology*, *286*, 94–108. <https://doi.org/10.1016/j.chemgeo.2011.04.007>
- Beaumais, A., Chazot, G., Dosso, L., & Bertrand, H. (2013). Temporal source evolution and crustal contamination at Lopevi Volcano, Vanuatu island arc. *Journal of Volcanology and Geothermal Research*, *263*, 72–84. <https://doi.org/10.1016/j.jvolgeores.2013.07.005>
- Beier, C., Brandl, P. A., Lima, S. L., & Haase, K. M. (2018). Tectonic control on the genesis of magmas in the New Hebrides arc (Vanuatu). *Lithos*, *312–313*, 290–307. <https://doi.org/10.1016/j.lithos.2018.05.011>
- Bellon, H., Marcelot, G., Lefèvre, C., & Maillet, P. (1984). Le volcanisme de l'île d'Erromango (République de Vanuatu): Calendrier de l'activité (données <sup>40</sup>K-<sup>40</sup>Ar). *Comptes Rendus Academie des Sciences Paris, Series II*, *299*, 257–262. [https://doi.org/10.1016/s1631-0713\(03\)00061-0](https://doi.org/10.1016/s1631-0713(03)00061-0)
- Ben Othman, D., White, W. M., & Patchett, J. (1989). The geochemistry of marine sediments, island arc magma genesis, and crust-mantle recycling. *Earth and Planetary Science Letters*, *94*, 1–21. [https://doi.org/10.1016/0012-821x\(89\)90079-4](https://doi.org/10.1016/0012-821x(89)90079-4)
- Bergeot, N., Bouin, M. N., Diament, M., Pelletier, B., Régner, M., Calmant, S., & Ballu, V. (2009). Horizontal and vertical interseismic velocity fields in the Vanuatu subduction zone from GPS measurements: Evidence for a central Vanuatu locked zone. *Journal of Geophysical Research*, *114*, B06405. <https://doi.org/10.1029/2007JB005249>
- Billen, M. I. (2017). Insights into the causes of arc rifting from 2-D dynamic models of subduction. *Geophysical Research Letters*, *44*, 10,948–10,957. <https://doi.org/10.1002/2017GL075061>
- Brandl, P. A., Beier, C., Regelous, M., Abouchami, W., Haase, K. M., Garbe-Schönberg, D., & Galer, S. J. G. (2012). Volcanism on the flanks of the East Pacific Rise: Quantitative constraints on mantle heterogeneity and melting processes. *Chemical Geology*, *298–299*, 41–56. <https://doi.org/10.1016/j.chemgeo.2011.12.015>
- Brenan, J. M., Shaw, H. F., & Ryerson, F. J. (1995). Experimental evidence for the origin of lead enrichment in convergent-margin magmas. *Nature*, *378*(6552), 54–56. <https://doi.org/10.1038/378054a0>
- Briqueu, L., Laporte, C., Crawford, A. J., Hasenaka, T., Baker, P. E., & Coltorti, M. (1994). Temporal magmatic evolution of the Aoba Basin, Central New Hebrides Island Arc: Pb, Sr, and Nd isotopic evidence for the coexistence of two mantle components beneath the arc. *Proceeding of the Ocean Drilling Program, Scientific Results*, *134*, 393–401. <https://doi.org/10.2973/odp.proc.sr.134.019.1994>
- Cagnioncle, A.-M., Parmentier, E. M., & Elkins-Tanton, L. T. (2007). Effect of solid flow above a subducting slab on water distribution and melting at convergent plate boundaries. *Journal of Geophysical Research*, *112*, B09402. <https://doi.org/10.1029/2007JB004934>
- Caratori Tontini, F., Bassett, D., de Ronde, C. E. J., Timm, C., & Wysoczanski, R. J. (2019). Early evolution of a young back-arc basin in the Havre Trough. *Nature Geoscience*, *12*(10), 856–862. <https://doi.org/10.1038/s41561-019-0439-y>
- Castillo, P. R., Lonsdale, P. F., Moran, C. L., & Hawkins, J. W. (2009). Geochemistry of Mid-Cretaceous Pacific crust being subducted along the Tonga-Kermadec Trench: Implications for the generation of arc lavas. *Lithos*, *112*(1–2), 87–102. <https://doi.org/10.1016/j.lithos.2009.03.041>
- Coltorti, M., Baker, P. E., Briqueu, L., Hasenaka, T., & Galassi, B. (1994). Petrology and geochemistry of volcanic rocks from the New Hebrides forearc region, sites 827, 829, and 830. *Proceeding of the Ocean Drilling Program, Scientific Results*, *134*, 337–352. <https://doi.org/10.2973/odp.proc.sr.134.015.1994>
- Compston, W., & Oversby, V. (1969). Lead isotopic analysis using a double spike. *Journal of Geophysical Research*, *74*(17), 4338–4348. <https://doi.org/10.1029/JB074i017p04338>
- Conger, J. A., Wiens, D. A., & Morris, J. (2002). On the decompression melting structure at volcanic arcs and back-arc spreading centers. *Geophysical Research Letters*, *29*, 1711–1714. <https://doi.org/10.1029/2002GL015390>

- Crawford, A. J., Briquieu, L., Laporte, C., & Hasenaka, T. (1995). Coexistence of Indian and Pacific oceanic upper mantle reservoirs beneath the Central New Hebrides island arc. In B. Taylor, & J. Natland (Eds.), *Active margins and marginal basins of the Western Pacific* (pp. 199–217). Washington, D.C.: American Geophysical Union, Geophysical Monograph
- Dupuy, C., Dostal, J., Marcelot, G., Bougault, H., Joron, J. L., & Treuil, M. (1982). Geochemistry of basalts from central and southern New Hebrides arc: Implication for their source rock composition. *Earth and Planetary Science Letters*, *60*, 207–225. [https://doi.org/10.1016/0012-821x\(82\)90004-8](https://doi.org/10.1016/0012-821x(82)90004-8)
- Eggins, S. M. (1993). Origin and differentiation of picritic arc magmas, Ambae (Aoba), Vanuatu. *Contributions to Mineralogy and Petrology*, *114*(1), 79–100. <https://doi.org/10.1007/BF00307867>
- Eissen, J.-P., Lefèvre, C., Maillat, P., Morvan, G., & Nohara, M. (1991). Petrology and geochemistry of the central North Fiji Basin spreading centre (Southwest Pacific) between 16°S and 22°S. *Marine Geology*, *98*(2-4), 201–239. [https://doi.org/10.1016/0025-3227\(91\)90104-C](https://doi.org/10.1016/0025-3227(91)90104-C)
- Eissen, J.-P., Nohara, M., Cotten, J., & Hirose, K. (1994). North Fiji Basin basalts and their magma sources: Part I. Incompatible element constraints. *Marine Geology*, *116*(1-2), 153–178. [https://doi.org/10.1016/0025-3227\(94\)90174-0](https://doi.org/10.1016/0025-3227(94)90174-0)
- Gerya, T. V. (2011). Future directions in subduction modeling. *Journal of Geodynamics*, *52*(5), 344–378. <https://doi.org/10.1016/j.jog.2011.06.005>
- Gerya, T. V., & Yuen, D. A. (2003). Rayleigh-Taylor instabilities from hydration and melting propel “cold plumes” at subduction zones. *Earth and Planetary Science Letters*, *212*, 47–62. [https://doi.org/10.1016/s0012-821x\(03\)00265-6](https://doi.org/10.1016/s0012-821x(03)00265-6)
- Gorton, M. P. (1977). The geochemistry and origin of quaternary volcanism in the New Hebrides. *Geochimica et Cosmochimica Acta*, *41*(9), 1257–1270. [https://doi.org/10.1016/0016-7037\(77\)90071-0](https://doi.org/10.1016/0016-7037(77)90071-0)
- Greene, H. G., & Collot, J.-Y. (1994). Ridge-arc collision: Timing and deformation determined by Leg 134 drilling, Central New Hebrides island arc. *Proceeding of the Ocean Drilling Program, Scientific Results*, *134*, 609–621. <https://doi.org/10.2973/odp.proc.sr.134.040.1994>
- Greene, H. G., Collot, J.-Y., Fisher, M. A., & Crawford, A. J. (1994). Neogene tectonic evolution of the New Hebrides island arc: A review incorporating ODP drilling results. *Proceeding of the Ocean Drilling Program, Scientific Results*, *134*, 19–46. <https://doi.org/10.2973/odp.proc.sr.134.002.1994>
- Grove, T. L., Till, C. B., & Krawczynski, M. J. (2012). The role of H<sub>2</sub>O in subduction zone magmatism. *Annual Review of Earth and Planetary Sciences*, *40*(1), 413–439. <https://doi.org/10.1146/annurev-earth-042711-105310>
- Haase, K. M., Regelous, M., Schöbel, S., Günther, T., & de Wall, H. (2019). Variation of melting processes and magma sources of the early Deccan flood basalts, Malwa Plateau, India. *Earth and Planetary Science Letters*, *524*, 115711. <https://doi.org/10.1016/j.epsl.2019.115711>
- Hall, P. S., Cooper, L. B., & Plank, T. (2012). Thermochemical evolution of the sub-arc mantle due to back-arc spreading. *Journal of Geophysical Research*, *117*, B02201. <https://doi.org/10.1029/2011JB008507>
- Hall, P. S., & Kincaid, C. (2001). Diapiric flow at subduction zones: A recipe for rapid transport. *Science*, *292*(5526), 2472–2475. <https://doi.org/10.1126/science.1060488>
- Hasenclever, J., Phipps Morgan, J., Hort, M., & Rüpke, L. H. (2011). 2D and 3D numerical models on compositionally buoyant diapirs in the mantle wedge. *Earth and Planetary Science Letters*, *311*(1–2), 53–68. <https://doi.org/10.1016/j.epsl.2011.08.043>
- Hayes, G. P., Wald, D. J., & Johnson, R. L. (2012). Slab 1.0: A three-dimensional model of global subduction zone geometries. *Journal of Geophysical Research*, *117*, B01302. <https://doi.org/10.1029/2011JB008524>
- Hermann, J., & Rubatto, D. (2009). Accessory phase control on the trace element signature of sediment melts in subduction zones. *Chemical Geology*, *265*(3–4), 512–526. <https://doi.org/10.1016/j.chemgeo.2009.05.018>
- Heuret, A., & Lallemand, S. (2005). Plate motions, slab dynamics and back-arc deformation. *Physics of the Earth and Planetary Interiors*, *149*(1–2), 31–51. <https://doi.org/10.1016/j.pepi.2004.08.022>
- Heyworth, Z., Knesel, K. M., Turner, S. P., & Arculus, R. J. (2011). Pb-isotopic evidence for rapid trench-parallel mantle flow beneath Vanuatu. *Journal of the Geological Society of London*, *168*(1), 265–271. <https://doi.org/10.1144/0016-76492010-054>
- Hochstaedter, A. G., Gill, J. B., & Morris, J. D. (1990). Volcanism in the Sumisu Rift, II. Subduction and non-subduction related components. *Earth and Planetary Science Letters*, *100*, 195–209. [https://doi.org/10.1016/0012-821x\(90\)90185-z](https://doi.org/10.1016/0012-821x(90)90185-z)
- Hofmann, A. W. (2003). Sampling mantle heterogeneity through oceanic basalts: Isotopes and trace elements. In *Treatise on Geochemistry* (pp. 61–101). Amsterdam: Elsevier.
- Ibrahim, A. K., Pontoise, B., Latham, G., Larue, M., Chen, T., Isacks, B., et al. (1980). Structure of the New Hebrides arc-trench system. *Journal of Geophysical Research*, *85*(B1), 253–266. <https://doi.org/10.1029/JB085iB01p00253>
- Ishibashi, J.-I., Wakita, H., Nojiri, Y., Grimaud, D., Jean-Baptiste, P., Gamo, T., et al. (1994). Helium and carbon geochemistry of hydrothermal fluids from the North Fiji Basin spreading ridge (southwest Pacific). *Earth and Planetary Science Letters*, *128*(3–4), 183–197. [https://doi.org/10.1016/0012-821x\(94\)90144-9](https://doi.org/10.1016/0012-821x(94)90144-9)
- Jicha, B. R., & Kay, S. M. (2018). Quantifying arc migration and the role of forearc subduction erosion in the central Aleutians. *Journal of Volcanology and Geothermal Research*, *360*, 84–99. <https://doi.org/10.1016/j.jvolgeores.2018.06.016>
- Karig, D. E. (1974). Evolution of arc systems in the western Pacific. *Annual Review of Earth and Planetary Sciences*, *2*(1), 51–75. <https://doi.org/10.1146/annurev.ea.02.050174.000411>
- Kempton, P. D., Pearce, J. A., Barry, T. L., Fitton, J. G., Langmuir, C., & Christie, D. M. (2002). Sr-Nd-Pb-Hf isotope results from ODP Leg 187: Evidence for mantle dynamics of the Australian-Antarctic discordance and origin of the Indian MORB source. *Geochemistry, Geophysics, Geosystems*, *3*(10). <https://doi.org/10.1029/2002GC000320>
- Kessel, R., Schmidt, M. W., Ulmer, P., & Pettke, T. (2005). Trace element signature of subduction-zone fluids, melts and supercritical liquids at 120–180 km depth. *Nature*, *437*(7059), 724–727. <https://doi.org/10.1038/nature03971>
- Kim, J., Lee, I., Halbach, P., Lee, K.-Y., Ko, Y.-T., & Kim, K.-H. (2006). Formation of hydrothermal vents in the North Fiji Basin: Sulfur and lead isotope constraints. *Chemical Geology*, *233*(3–4), 257–275. <https://doi.org/10.1016/j.chemgeo.2006.03.011>
- Kincaid, C., & Hall, P. S. (2003). Role of back arc spreading in circulation and melting at subduction zones. *Journal of Geophysical Research*, *108*(B5), 2240. <https://doi.org/10.1029/2001JB001174>
- Koppers, A. A. P. (2002). ArArCALC—Software for <sup>40</sup>Ar/<sup>39</sup>Ar age calculations. *Computers and Geosciences*, *28*(5), 605–619. [https://doi.org/10.1016/S0098-3004\(01\)00095-4](https://doi.org/10.1016/S0098-3004(01)00095-4)
- Koppers, A. A. P., Russell, J. A., Roberts, J., Jackson, M. G., Konter, J. G., Wright, D. J., et al. (2011). Age systematics of two young en echelon Samoan volcanic trails. *Geochemistry, Geophysics, Geosystems*, *12*, Q07025. <https://doi.org/10.1029/2010GC003438>
- Kuiper, K. F., Deino, A., Hilgen, F. J., Krijgsman, F. J., Renne, P. R., & Wijbrans, J. (2008). Synchronizing rock clocks of Earth history. *Science*, *320*(5875), 500–504. <https://doi.org/10.1126/science.1154339>
- Kushiro, I. (1990). Partial melting of mantle wedge and evolution of island arc crust. *Journal of Geophysical Research*, *95*(B10), 15,929–15,939. <https://doi.org/10.1029/JB095iB10p15929>

- Lagabrielle, Y., Goslin, J., Martin, H., Thiriot, J.-L., & Auzende, J.-M. (1997). Multiple active spreading centres in the hot North Fiji Basin (Southwest Pacific): A possible model for Archean seafloor dynamics? *Earth and Planetary Science Letters*, *149*, 1–13. [https://doi.org/10.1016/S0012-821X\(97\)00060-5](https://doi.org/10.1016/S0012-821X(97)00060-5)
- Laporte, C., Briquieu, L., Cluzel, D., & Eissen, J.-P. (1998). Isotopic gradient along the New Hebrides arc (Vanuatu, SW Pacific). Collision of the d'Entrecasteaux Zone and heterogeneity of mantle sources. *Comptes Rendus Academie des Sciences Paris, Sciences de la Terre et des planètes*, *326*, 101–106. [https://doi.org/10.1016/S1251-8050\(97\)87453-8](https://doi.org/10.1016/S1251-8050(97)87453-8)
- Lima, S. M., Haase, K. M., Beier, C., Regelous, M., Brandl, P. A., Hauff, F., & Krumm, S. (2017). Magmatic evolution and source variations at the Nifonea Ridge (New Hebrides Island Arc). *Journal of Petrology*, *58*(3), 473–494. <https://doi.org/10.1093/petrology/egx023>
- Maillet, P., Ruellan, E., Gérard, M., Person, A., Bellon, H., Cotten, J., et al. (1995). Tectonics, magmatism, and evolution of the New Hebrides backarc troughs (Southwest Pacific). In B. Taylor (Ed.), *Backarc basins: tectonics and magmatism* (pp. 177–235). New York: Plenum Press. [https://doi.org/10.1007/978-1-4615-1843-3\\_5](https://doi.org/10.1007/978-1-4615-1843-3_5)
- Marcelot, G., Maury, R. C., & Lefevre, C. (1983). Mineralogy of Erromango lavas (New Hebrides): Evidence of an early stage of fractionation in island arc basalts. *Lithos*, *16*(2), 135–151. [https://doi.org/10.1016/0024-4937\(83\)90011-7](https://doi.org/10.1016/0024-4937(83)90011-7)
- Martinez, F., & Taylor, B. (2006). Modes of crustal accretion in back-arc basins: Inferences from the Lau Basin. In *Back-arc spreading systems: Geological, biological, chemical, and physical interactions* (pp. 5–29). Washington, D.C.: American Geophysical Union. <https://doi.org/10.1029/166GM03>
- McConachy, T. F., Arculus, R. J., Yeats, C. J., Binns, R. A., Barriga, F. J. A. S., McInnes, B. I. A., et al. (2005). New hydrothermal activity and alkalic volcanism in the backarc Coriolis Troughs Vanuatu. *Geology*, *33*(1), 61–64. <https://doi.org/10.1130/G20870.1>
- McCulloch, M. T., & Gamble, J. A. (1991). Geochemical and geodynamical constraints on subduction zone magmatism. *Earth and Planetary Science Letters*, *102*(3–4), 358–374. [https://doi.org/10.1016/0012-821X\(91\)90029-H](https://doi.org/10.1016/0012-821X(91)90029-H)
- Métrich, N., Allard, P., Aiuppa, A., Bani, P., Bertagnini, A., Shinohara, H., et al. (2011). Magma and volatile supply to post-collapse volcanism and block resurgence in Siwi Caldera (Tanna Island, Vanuatu Arc). *Journal of Petrology*, *52*(6), 1077–1105. <https://doi.org/10.1093/petrology/egr019>
- Min, K. W., Mundil, R., Renne, P. R., & Ludwig, K. R. (2000). A test for systematic errors in  $^{40}\text{Ar}/^{39}\text{Ar}$  geochronology through comparison with U/Pb analysis of a 1.1-Ga rhyolite. *Geochimica et Cosmochimica Acta*, *64*(1), 73–98. [https://doi.org/10.1016/S0016-7037\(99\)00204-5](https://doi.org/10.1016/S0016-7037(99)00204-5)
- Molnar, P., & Atwater, T. (1978). Interarc spreading and Cordilleran tectonics as alternates related to the age of subducted oceanic lithosphere. *Earth and Planetary Science Letters*, *41*, 330–340. [https://doi.org/10.1016/0012-821X\(78\)90187-5](https://doi.org/10.1016/0012-821X(78)90187-5)
- Monjaret, M. J., Bellon, H., & Maillet, P. (1991). Magmatism of the troughs behind the New Hebrides island arc (RV Jean Charcot SEAPSO 2 cruise): K-Ar geochronology and petrology. *Journal of Volcanology and Geothermal Research*, *46*(3–4), 265–280. [https://doi.org/10.1016/0377-0273\(91\)90088-H](https://doi.org/10.1016/0377-0273(91)90088-H)
- Monzier, M., Robin, C., Eissen, J.-P., & Cotten, J. (1997). Geochemistry vs. seismo-tectonics along the volcanic New Hebrides Central Chain (Southwest Pacific). *Journal of Volcanology and Geothermal Research*, *78*(1–2), 1–29. [https://doi.org/10.1016/S0377-0273\(97\)00006-1](https://doi.org/10.1016/S0377-0273(97)00006-1)
- Mortimer, N., Gans, P. B., Meffre, S., Martin, C. E., Seton, M., Williams, S., et al. (2018). Regional volcanism of northern Zealandia: Post-Gondwana break-up magmatism on an extended, submerged continent. In S. Sensarma, & B. C. Storey (Eds.), *Large igneous provinces from Gondwana and adjacent regions* (pp. 199–226). London: Geol. Soc. London, Spec. Publ.
- Mortimer, N., Gans, P. B., Palin, J. M., Herzer, R. H., Pelletier, B., & Monzier, M. (2014). Eocene and Oligocene basins and ridges of the Coral Sea-New Caledonia region: Tectonic link between Melanesia, Fiji, and Zealandia. *Tectonics*, *33*(7), 1386–1407. <https://doi.org/10.1002/2014TV003598>
- Mortimer, N., Herzer, R. H., Gans, P. B., Laporte-Magoni, C., Calvert, A. T., & Bosch, D. (2007). Oligocene-Miocene tectonic evolution of the South Fiji Basin and Northland Plateau, SW Pacific Ocean: Evidence from petrology and dating of dredged rocks. *Marine Geology*, *237*(1–2), 1–24. <https://doi.org/10.1016/j.margeo.2006.10.033>
- Mortimer, N., Herzer, R. H., Gans, P. B., Parkinson, D. L., & Seward, D. (1998). Basement geology from Three Kings Ridge to West Norfolk Ridge, southwest Pacific Ocean: Evidence from petrology, geochemistry and isotopic dating of dredge samples. *Marine Geology*, *148*(3–4), 135–162. [https://doi.org/10.1016/S0025-3227\(98\)00007-3](https://doi.org/10.1016/S0025-3227(98)00007-3)
- Nishio, Y., Sasaki, S., Gamo, T., Hiyagon, H., & Sano, Y. (1998). Carbon and helium isotope systematics of North Fiji Basin basalt glasses: Carbon geochemical cycle in the subduction zone. *Earth and Planetary Science Letters*, *154*, 127–138. [https://doi.org/10.1016/S0012-821X\(97\)00187-8](https://doi.org/10.1016/S0012-821X(97)00187-8)
- Nohara, M., Hirose, K., Eissen, J.-P., Urabe, T., & Joshima, M. (1994). The North Fiji Basin basalts and their magma sources: Part II. Sr-Nd isotopic and trace element constraints. *Marine Geology*, *116*(1–2), 179–195. [https://doi.org/10.1016/0025-3227\(94\)90175-9](https://doi.org/10.1016/0025-3227(94)90175-9)
- Packham, G. H., & Andrews, J. E. (1975). Results of Leg 30 and the geologic history of the Southwest Pacific arc and marginal sea complex. *Initial Reports of the Deep Sea Drilling Project*, *30*, 691–705. <https://doi.org/10.2973/dsdp.proc.30.126.1975>
- Pearce, J. A. (2005). Mantle preconditioning by melt extraction during flow: Theory and petrogenetic implications. *Journal of Petrology*, *46*(5), 973–997. <https://doi.org/10.1093/petrology/egi007>
- Pearce, J. A., Ernewein, M., Bloomer, S. H., Parson, L. M., Murton, B. J., & Johnson, L. E. (1995). Geochemistry of Lau Basin volcanic rocks: Influence of ridge segmentation and arc proximity. In J. L. Smellie (Ed.), *Volcanism associated with extension at consuming plate margins* (pp. 53–75). London: Geol. Soc. Spec. Vol.
- Pearce, J. A., Kempton, P. D., & Gill, J. B. (2007). Hf-Nd evidence for the origin and distribution of mantle domains in the SW Pacific. *Earth and Planetary Science Letters*, *260*, 98–114. <https://doi.org/10.1016/j.epsl.2007.05.023>
- Peate, D. W., Pearce, J. A., Hawkesworth, C. J., Colley, H., Edwards, C. M. H., & Hirose, K. (1997). Geochemical variations in Vanuatu Arc lavas: The role of subducted material and a variable mantle wedge composition. *Journal of Petrology*, *38*(10), 1331–1358. <https://doi.org/10.1093/ptro/38.10.1331>
- Pelletier, B., Calmant, S., & Pillot, R. (1998). Current tectonics of the Tonga-New Hebrides region. *Earth and Planetary Science Letters*, *164*, 263–276. [https://doi.org/10.1016/S0012-821X\(98\)00212-X](https://doi.org/10.1016/S0012-821X(98)00212-X)
- Plank, T., & Langmuir, C. H. (1993). Tracing trace elements from sediment input to volcanic output at subduction zones. *Nature*, *362*(6422), 739–743. <https://doi.org/10.1038/362739a0>
- Raos, A. M., & Crawford, A. J. (2004). Basalts from the Efate Island Group, central section of the Vanuatu arc, SW Pacific: Geochemistry and petrogenesis. *Journal of Volcanology and Geothermal Research*, *134*(1–2), 35–56. <https://doi.org/10.1016/j.jvolgeores.2003.12.004>
- Robin, C., Eissen, J.-P., & Monzier, M. (1994). Ignimbrites of basaltic andesite and andesite compositions from Tanna, New Hebrides Arc. *Bulletin of Volcanology*, *56*(1), 10–22. <https://doi.org/10.1007/BF00279725>
- Romer, R. L., Förster, H.-J., & Breitrkreuz, C. (2001). Intracontinental extensional magmatism with a subduction fingerprint: The late carboniferous Halle Volcanic Complex (Germany). *Contributions to Mineralogy and Petrology*, *141*(2), 201–221. <https://doi.org/10.1007/s004100000231>

- Saunders, A. D., & Tarney, J. (1979). The geochemistry of basalts from a back-arc spreading centre in the East Scotia Sea. *Geochimica et Cosmochimica Acta*, 43(4), 555–572. [https://doi.org/10.1016/0016-7037\(79\)90165-0](https://doi.org/10.1016/0016-7037(79)90165-0)
- Schellart, W. P. (2008). Subduction zone trench migration: Slab driven or overriding-plate-driven? *Physics of the Earth and Planetary Interiors*, 170(1–2), 73–88. <https://doi.org/10.1016/j.pepi.2008.07.040>
- Schellart, W. P., Lister, G. S., & Toy, V. G. (2006). A Late Cretaceous and Cenozoic reconstruction of the Southwest Pacific region: Tectonics controlled by subduction and slab rollback processes. *Earth Science Reviews*, 76(3–4), 191–233. <https://doi.org/10.1016/j.earscirev.2006.01.002>
- Schmidt, K., Garbe-Schönberg, D., Hannington, M. D., Anderson, M. O., Bühring, B., Haase, K., et al. (2017). Boiling vapour-type fluids from the Nifonea vent field (New Hebrides Back-Arc, Vanuatu, SW Pacific): Geochemistry of an early-stage, post-eruptive hydrothermal system. *Geochimica et Cosmochimica Acta*, 207, 185–209. <https://doi.org/10.1016/j.gca.2017.03.016>
- Sdrolias, M., Müller, R. D., & Gaina, C. (2003). Tectonic evolution of the southwest Pacific using constraints from backarc basins. *Geological Society of Australia Special Publications*, 22, 343–359. <https://doi.org/10.1130/0-8137-2372-8.343>
- Shinjo, R., Chung, S.-L., Kato, Y., & Kimura, M. (1999). Geochemical and Sr-Nd isotopic characteristics of volcanic rocks from the Okinawa Trough and Ryukyu Arc: Implications for the evolution of a young, intracontinental back arc basin. *Journal of Geophysical Research*, 104(B5), 10,591–10,608. <https://doi.org/10.1029/1999JB900040>
- Sleep, N. H., & Toksöz, M. N. (1971). Evolution of marginal basins. *Nature*, 33, 548–550. <https://doi.org/10.1038/233548a0>
- Sleeper, J. D., & Martinez, F. (2014). Controls on segmentation and morphology along the back-arc Eastern Lau Spreading Center and Valu Fa Ridge. *Journal of Geophysical Research*, 119, 1678–1700. <https://doi.org/10.1002/2013JB010545>
- Sorbadere, F., Schiano, P., Métrich, N., & Bertagnini, A. (2013). Small-scale coexistence of island-arc- and enriched-MORB-type basalts in the central Vanuatu arc. *Contributions to Mineralogy and Petrology*, 166(5), 1305–1321. <https://doi.org/10.1007/s00410-013-0928-8>
- Spandler, C., Mavrogenes, J., & Hermann, J. (2007). Experimental constraints on element mobility from subducted sediments using high-P synthetic fluid/melt inclusions. *Chemical Geology*, 239(3–4), 228–249. <https://doi.org/10.1016/j.chemgeo.2006.10.005>
- Steiger, R. H., & Jäger, E. (1977). Subcommittee on geochronology: Convention on the use of decay constants in geo- and cosmochemistry. *Earth and Planetary Science Letters*, 36, 359–362. [https://doi.org/10.1016/0012-821x\(77\)90060-7](https://doi.org/10.1016/0012-821x(77)90060-7)
- Sun, S.-S., & McDonough, W. F. (1989). Chemical and isotopic systematics of oceanic basalts: Implications for mantle composition and processes. In A. D. Saunders, & M. J. Norry (Eds.), *Magmatism in the ocean basins* (pp. 313–345). London: Geology Society Special Publications.
- Syracuse, E. M., & Abers, G. A. (2006). Global compilation of variations in slab depth beneath arc volcanoes and implications. *Geochemistry, Geophysics, Geosystems*, 7, Q05017. <https://doi.org/10.1029/2005GC001045>
- Tamaki, K. (1985). Two modes of back-arc spreading. *Geology*, 13(7), 475–478. [https://doi.org/10.1130/0091-7613\(1985\)13<475:TMOBS>2.0.CO;2](https://doi.org/10.1130/0091-7613(1985)13<475:TMOBS>2.0.CO;2)
- Taylor, B. E., Klaus, A., Brown, G. R., Moore, G. F., Okamura, Y., & Murakami, F. (1991). Structural development of Sumisu Rift, Izu-Bonin Arc. *Journal of Geophysical Research*, 96(B10), 16,113–16,129. <https://doi.org/10.1029/91JB01900>
- Taylor, J. R. (1997). *An introduction to error analysis: The study of uncertainties in physical measurements* (pp. 327). Sausalito, USA: Scion Publishing.
- Todd, E., Gill, J. B., Wysoczanski, R. J., Hergt, J., Wright, I. C., Leybourne, M. I., & Mortimer, N. (2011). Hf isotopic evidence for small-scale heterogeneity in the mode of mantle wedge enrichment: Southern Havre Trough and South Fiji Basin back arcs. *Geochemistry, Geophysics, Geosystems*, 11, Q04009. <https://doi.org/10.1029/2009GC002888>
- Trua, T., Clocchiatti, R., Schiano, P., Ottolini, L., & Marani, M. (2010). The heterogeneous nature of the Southern Tyrrhenian mantle: Evidence from olivine-hosted melt inclusions from back-arc magmas of the Marsili seamount. *Lithos*, 118(1–2), 1–16. <https://doi.org/10.1016/j.lithos.2010.03.008>
- Turner, S. P., Peate, D. W., Hawkesworth, C. J., Eggins, S. M., & Crawford, A. J. (1999). Two mantle domains and the time scales of fluid transfer beneath the Vanuatu arc. *Geology*, 27(11), 963–966. [https://doi.org/10.1130/0091-7613\(1999\)027<0963:TMDATT>2.3.CO;2](https://doi.org/10.1130/0091-7613(1999)027<0963:TMDATT>2.3.CO;2)
- Uyeda, S., & Kanamori, H. (1979). Back-arc opening and the mode of subduction. *Journal of Geophysical Research*, 84(B3), 1049–1061. <https://doi.org/10.1029/JB084iB03p01049>
- van Keken, P. E., Hacker, B. R., Syracuse, E. M., & Abers, G. A. (2011). Subduction factory: 4. Depth-dependent flux of H<sub>2</sub>O from subduction slabs worldwide. *Journal of Geophysical Research*, 116, B01401. <https://doi.org/10.1029/2010JB007922>
- Wallace, L. M., Ellis, S., & Mann, P. (2009). Collisional model for rapid fore-arc block rotations, arc curvature, and episodic back-arc rifting in subduction settings. *Geochemistry, Geophysics, Geosystems*, 10, Q05001. <https://doi.org/10.1029/2008GC002220>
- Wiens, D. A., Conder, J. A., & Faul, U. H. (2008). The seismic structure and dynamics of the mantle wedge. *Annual Review of Earth and Planetary Sciences*, 36(1), 421–455. <https://doi.org/10.1146/annurev.earth.33.092203.122633>
- Wilson, C. R., Spiegelman, M., van Keken, P. E., & Hacker, B. R. (2014). Fluid flow in subduction zones: The role of solid rheology and compaction pressure. *Earth and Planetary Science Letters*, 401, 261–274. <https://doi.org/10.1016/j.epsl.2014.05.052>
- Woodhead, J., Eggins, S., & Gamble, J. (1993). High field strength and transition element systematics in island arc and back-arc basin basalts: Evidence for multi-phase melt extraction and a depleted mantle wedge. *Earth and Planetary Science Letters*, 114, 491–504. [https://doi.org/10.1016/0012-821X\(93\)90078-N](https://doi.org/10.1016/0012-821X(93)90078-N)
- Workman, R. K., & Hart, S. R. (2005). Major and trace element composition of the depleted MORB mantle (DMM). *Earth and Planetary Science Letters*, 231, 53–72. <https://doi.org/10.1016/j.epsl.2004.12.005>
- York, D. (1968). Least squares fitting of a straight line with correlated errors. *Earth and Planetary Science Letters*, 5, 320–324. [https://doi.org/10.1016/S0012-821X\(68\)80059-7](https://doi.org/10.1016/S0012-821X(68)80059-7)
- Zhang, N., & Pysklywec, R. N. (2006). Role of mantle flow at the North Fiji Basin: Insights from anomalous topography. *Geochemistry, Geophysics, Geosystems*, 7, Q12002. <https://doi.org/10.1029/2006GC001376>